KATHMANDU UNIVERSITY
SCHOOL OF ENGINEERING
DEPARTMENT OF MECHANICAL ENGINEERING

FINAL REPORT ON

DESIGN OPTIMIZATION OF FRANCIS TURBINE RUNNER BLADES AT FIXED GUIDE VANE OPENING

In Partial Fulfillment of the Requirements for the
Bachelor's Degree in Mechanical Engineering

Bibek Giri [42257]
Nikshan Paudel [42268]

November 2019

AUTHORIZATION

We hereby declare that we are the sole author of the project.

We authorize Kathmandu University to lend this project report to other institutions or individuals for the purpose of scholarly research. We further authorize the university to reproduce the report by photocopying or by other means, in total or in part, at the request of other institutions or individuals for the purpose of scholarly research.

_____

Bibek Giri

_____

Nikshan Paudel

November 2019

PROJECT EVALUATION

Design Optimization of Francis Turbine Runner Blades at Fixed Guide Vane Opening

by

Bibek Giri

Nikshan Paudel

This is to certify that I have examined the above Project report and have found that it is complete and satisfactory in all respects, and that any and all revisions required by the report examination committee have been made.

Associate Professor Dr. Rajendra Shrestha	Asst. Prof. Dr. Biraj Singh Thapa
External Examiner	Supervisor
Institute of Engineering (IOE), Pulchowk	Department of Mechanical Engineering
Dr. Sailesh Chitrakar	Er. Dadi Ram Dahal
Co-supervisor	Co-supervisor
Department of Mechanical Engineering	Department of Mechanical Engineering

Associate Professor Dr. Daniel Tuladhar

Head of Department

Department of Mechanical Engineering

November 2019

ACKNOWLEDGEMENT

We would like to thank our supervisor Dr. Biraj Singh Thapa for his continuos supervision and guidance from the inception of the work. We would also like to thank our co-supervisors Dr.Sailesh Chitrakar and Er .Dadi Ram Dahal for their guidance throughout the project. The work would not have been completed without their continuos efforts.

Sincere thanks to all TTL members for their support and time .Also, special thanks to Mr. Bhuwan Bhattarai, TTL technician for his work and help in the project.

Finally we would also like to thank the Department of Mechanical Engineering, KU for allowing to carry out this work.

ABSTRACT

This research thesis comprises of both the experimental studies and numerical simulation of a fixed guide vane Francis turbine. Experiments were conducted in a test rig available at Turbine Testing Laboratory, KU. CFD based design, performance analysis and design optimization are carried out in this study.

During the experiment, main pump setup is used to provide the required head and flow through the turbine. Electro-magnetic flow meter and pressure transducer are respectively used to measure the flow and pressure in the setup. The turbine was coupled with an induction motor through a torque transducer which was further driven by a VFD. Data logging was carried out using LabVIEW software. Experiments are conducted at various rpm and discharges.

Numerical simulations were carried out using CFD based ANSYS CFX 15.0 for single phase steady state with SST turbulence model. The design parameters include 16 m head, 0.1 m^3/s flow rate and 1500 rpm. Numerical results were compared to the experimental results. Several parameters affecting the efficiency of the Francis turbine were studied and design modifications were done to enhance the efficiency.

To enhance the efficiency of the turbine, various parameters are modified and their effects had been studied independently. Blade lean and Beta distribution in the blade had been changed to study their effects in the efficiency of the runner. Finally an optimized runner has been proposed after having no leading edge cavitation and better performance throughout the operating range.

TABLE OF CONTENTS

LIST OF FIGURES

LIST OF TABLES

LIST OF ABBREVIATIONS

TTL	Turbine Testing Laboratory
KU	Kathmandu University
CFD	Computational Fluid Dynamics
MATLAB	Mathematical Laboratory
MW	Megawatts
kW	Kilowatts
VFD	Variable Frequency Drive
ANSYS	Analysis Systems
RPM	Revolutions per minute
BSL	Baseline Model
SST	Shear Stress Transport
RANS	Reynolds Averaged Navier- Stokes
HP	Horse- Power

LIST OF SYMBOLS

H	Head	[m]
ŋ	Efficiency	[%]
ω	Angular velocity	[rad/s]
τ	Torque	[Nm]
g	Acceleration due to gravity	[m/s^2]
P	Power	[W]
Q	Flow rate	[m^3/s]
β	Angle between tangent of the blade and runner periphery	[^{o}]
ρ	Specific water density	[kg/m^3]
Ø	Speed ratio	[-]
π	Constant	[-]
ψ	Blade roughness coefficient	[-]
U	Peripheral Velocity of Runner	[m/s]

CHAPTER 1 INTRODUCTION

1.1 Background

The Francis turbine was invented by an American inventor James B. Francis in the 1800s. The Francis turbine is an inward flow reaction turbine and is used in devices with a wide variety of head and flow. The Francis Turbine is the most commonly used turbine today to generate hydroelectricity. They are often used in large hydroelectric dam systems. The Francis turbine is a versatile turbine that can be built with either a horizontal or vertical axis and can be used in many different hydraulic head heights and water flow levels. This turbine also uses mobile guide vanes to direct the water into the turbine which can be set to allow the desired level of water flow into the turbine system.

With about 60% of the global hydropower capacity in the world, Francis turbines are the most widely used type of hydro turbine. Francis turbines are very able to sustain the high mechanical stress resulting from high heads. They operate in a water head from 40 to 600 m and are primarily used for electrical power production. The electric generators which most often use this type of turbine have a power output which generally ranges just a few kilowatts up to 800 MW, though mini-hydro installations may be lower. Penstock (input pipes) diameters are between 3 and 33 feet (0.91 and 10.06 meters). The speed range of the turbine is from 75 to 1000 rpm. Wicket gates around the outside of the turbine's rotating runner control the rate of water flow through the turbine for different power production rates. Francis turbines are almost always mounted with the shaft vertical to isolate water from the generator. This also facilitates installation and maintenance.

Among all hydraulic turbine machines used for energy conversion, vast operating regime of Francis turbine enables it to be used for varying range of small to large hydro power plant. This makes Francis turbine most popular and hence it is used in maximum number of hydro power plants. In order to develop a reliable machine for this highly demanding operation, the behavior of the flow in the entire turbine regime has to be predicted by a reliable computational method like CFD which is a very economical method. The prediction of prototype turbine performance in actual prevailing conditions is very important for engineers. In order to know the feasibility of the turbine, it is essential to project the results in advance. Since turbines are tailor made as per the requirement of the prevailing site conditions, a unique performance prediction has to be made for a separate turbine. This can be done either by theoretical methods, experimental methods or by computational method (i.e. CFD). Among all methods CFD stands its unique

importance, since by this method study of the flow inside turbine space can be made. Flow pattern in intricate portions of the component can also be analyzed and variation of the results can be known with the varying conditions. CFD method consumes less money, less gestation period in comparison to the experimental method which requires model fabrication and test rig set up. CFD approach is a combination of numerical technique and computational power. With the help of CFD technique even complex flow pattern inside hydraulic turbine parts can be analyzed in detail and modifications can be implemented. It can be used for increasing the efficiency by making necessary modification in the design of hydraulic turbine and checking relevancy of alternate optimized design before the turbine is finally manufactured. However, in order to check the reliability of selected optimized design, validation of the results is to be done with experimental results. CFD technique has led to significant enhancement in efficiency of hydraulic turbine. CFD can also be used to check efficiency of alternate design of hydraulic turbine for optimization before final testing is done. To improve reliability of CFD technique, validations of results are required with experimental results. In present work Francis turbine considered with Horizontal axis. CFD analysis is done on varying working conditions and tabulations of results are done to get the clear picture of changes in the results.

The name MATLAB stands for Matrix Laboratory. MATLAB was written originally to provide easy access to matrix software developed by the LINPACK (linear system package) and EISPACK (Eigen system package) projects. MATLAB is a high-performance language for technical computing. It integrates computation, visualization, and programming environment. Furthermore, MATLAB is a modern programming language environment: it has sophisticated data structures, contains built-in editing and debugging tools, and supports object-oriented programming. These factors make MATLAB an excellent tool for teaching and research. MATLAB has many advantages compared to conventional computer languages (e.g. C, FORTRAN) for solving technical problems. MATLAB is an interactive system whose basic data element is an array that does not require dimensioning. The software package has been commercially available since 1984 and is now considered as a standard tool at most universities and industries worldwide. It has powerful built-in routines that enable a very wide variety of computations. It also has easy to use graphics commands that make the visualization of results immediately available. Special applications are collected in packages referred to as toolbox. There are toolboxes for signal processing, symbolic computation, control theory, simulation, optimization, and several other field of applied science and engineering.

1.2 Objective

Primary Objectives

1. To propose an optimized design of Francis runner at fixed guide vane opening.
2. To analyze the performance of runner through experimentation.

Secondary Objectives

1. To propose a design tool with consideration on parametric relations.

1.3 Scope

1. Experimentation was carried out for a reference case only.
2. Parametric study for change in efficiency was considered.
3. In-House MATLAB code was used for hydraulic design of the runner.
4. Parameters as blade lean, meridional shape and loading were studied.

1.4 Limitations

1. Experimental analysis of Optimized runner was not carried out.
2. Design tool incorporates hydraulic design only.
3. Performance analysis is limited to efficiency measurement only.

CHAPTER 2 METHODOLOGY

2.1 Literature review

In the design and development of Francis turbine various researches and works have been done to attain the desired efficient model of Francis turbine. Various design methods have been suggested and applied to obtain the Francis turbine. Various researches has been carried out in designing and optimization of Francis turbines. Some of the works of have been listed in this section.

Biraj Singh Thapa has proposed a new design philosophy of Francis turbine was conducted to minimize the sediment erosion effect with the help of design tool in MATLAB. Runner outlet diameter, peripheral velocity at inlet, and blade angle distribution had highest effect on sediment erosion of Francis runner. Parabolic blade angle distribution has been found to drop the erosion by almost 30%. Change in blade angle has no effects other than change in shape of blade and relative velocities. Change in shape of blade may have strength and manufacturing limitations. [1] Lars Froyd developed a design tool for the design of low head Francis turbine in which he found that an outward sloping turbine outlet geometry which may be seen in low-head Francis turbines, is still not possible to model due to numerical design approach. [2] Y Enomoto improved the hydraulic performance in a high specific speed Francis turbine runner through the combination of Computational Fluid Dynamics and a multi objective optimization and confirmed that the optimized runner presented higher efficiency compared to the originally designed runner. [3] Ujjwal Shrestha studied the effect of runner design parameters on 50 MW Francis hydro turbine model performance and optimized the runner through modifications of runner meridional shape (curve profile of hub, shroud, leading edge and trailing edge), blade angle and its distribution for the enhancement of performance. Blade loading had direct impact on performance and a better runner can be designed following a front loading profile. [4] Maciej Kaniecki performed CFD analysis of high speed Francis hydraulic turbines using two different Francis runners that mapped accurately with the performance of installed model turbine ensuring the use of CFD for exact prediction of behavior of the turbine. [5] Ayancik Fatma (2014) found parametric design based on numerical calculation indicates that hydraulic design parameters causes different effects on the blade shape and the turbine performance. Parametric relations between the beta and the theta angle shows that the beta angle distribution has an important role in the design process. [6]

Kazayuki Nakamura and Sadao Kurosawa (2009) optimized runner shape automatically enables on the constraints of the tradeoff relationship between the runner loss and the draft tube loss. The runner has great improvement on the turbine operating efficiency in the wide operating range. [7] Zhe Ma carried out a comprehensive hydraulic improvement and parametric analysis of a Francis runner and investigated to reveal the relationship with runner's internal flow and outer performances varying runners with different main design inputs, namely blade lean, blade loading and blade meridional shape. This optimization system supplied satisfactory results and convincing recommendations to determine the design inputs for low-head Francis turbine runners. Compared with the initial runner, the runner generated from this method had a satisfactory improvement. In detail, unit efficiencies of the preferred runner were increased by 0.91%, 0.47% and 0.37%, respectively, under the rated head, a high head and the maximum head. [8]

From these researches and works it has been clear that a significant increase in the efficiency and power output can be obtained by optimization of parameters. All these studies has led to the ease and necessity to carry out this research with much intent and dedication. So, this research focusses on design optimization of the runner through parametric study and their analysis.

.

2.2 Study Design

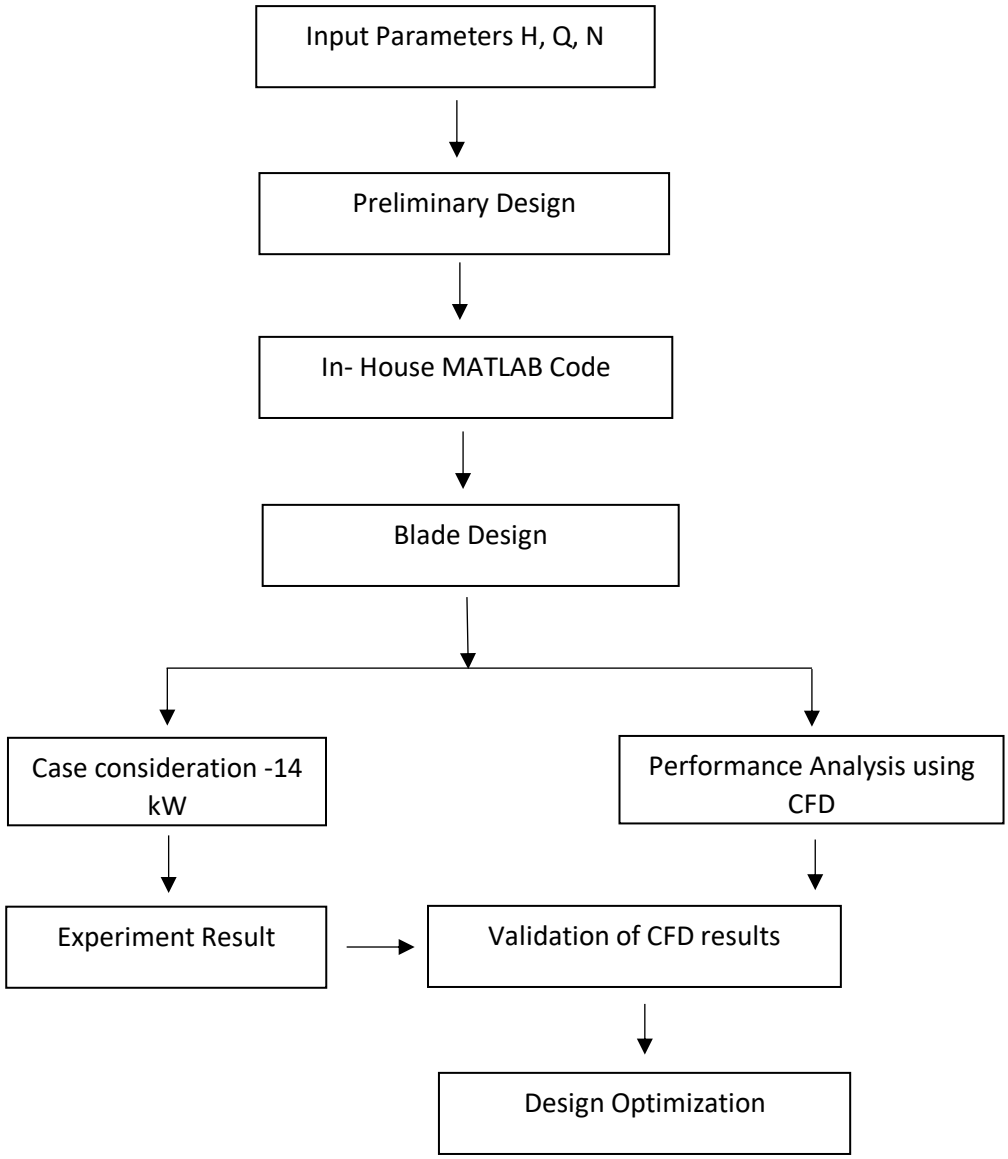

Design of Francis turbine runner will be done for a case reference of 14 kW using the In-House MATLAB code using Bovet approach of blade design. Performance analysis of the runner using CFD will be carried out to know the efficiencies variation at different discharges. The results of the simulation will be validated through the experimental results through a test carried at TTL, KU for a reference case. Experimental results and CFD results will be analyzed and interpreted.

Finally the design of reference case will be taken for optimization. Effect of blade lean and sweep will be considered. Effect of varying meridional shape and blade loading will be analyzed and an optimized runner design will be proposed along with its relation with various parameters.

In- House MATLAB code: A Francis turbine similar to Khoj has been developed to facilitate the design of Francis turbine at TTL, KU. It uses Bovet approach of blade design to design meridional view of the blade. It can export CS1V files of the runner blade, hub, shroud, spiral casing, guide vane, stay vane considering the input parameters.

CFD: CFD module is a numerical simulation platform for computational fluid dynamics that describes the fluid flow processes and engineering designs.
Francis turbine is a type of reaction turbine in which working fluid comes to the turbine under immense pressure and the energy is extracted by the turbine blades from the working fluid. A part of the energy is given up by the fluid because of pressure changes occurring in the blades of the turbine, quantified by the expression of degree of reaction, while the remaining part of the energy is extracted by the volute casing of the turbine. At the exit, water accts on the spinning cup-shaped runner features, leaving at low velocity and low swirl with very little kinetic or potential energy left. The turbine's exit tube is shaped to help decelerate the water flow and recover the pressure.

The fluid flow and the effects of varying various parameters of blade design will be considered and efficiency at every change will be plotted to find an optimum condition. Parametric study of runner will be done and optimized runner will be proposed.

Experimental Result: A 14 kW Francis turbine has been developed and will be tested at TTL. Performance of the runner will be analyzed. The experimental result analysis will shall validate the results of CFD in design of the runner. Parametric analysis of this runner has not been done which has led to the need of this project.

CHAPTER 3 HYDRAULIC DESIGN OF FRANCIS TURBINE

3.1 Bovet Method

Bovet simplified the design approach by introducing dimensionless specific speed and is given as in expression below:

$$n_0^* = \phi_{2e}^{1/2} \times \phi_{2e}^{-3/4} = \frac{\omega\left(\frac{Q}{\pi}\right)^{\frac{1}{2}}}{(2gH)^{\frac{3}{4}}} \tag{3.1}$$

All the dimensions of runner are now expressed in terms of this dimensionless number.

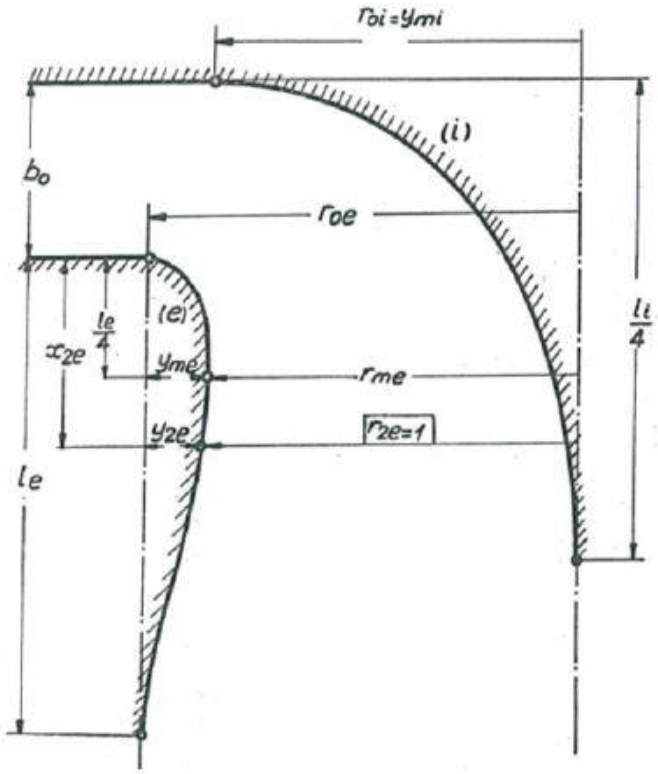

Figure 3.1 Meridional Parameters of Francis Turbine [9]

In above figure specific dimensions of runner is given which is obtained after dividing the dimensions by R_{2e}. R_{2e} is the distance between rotational axis of the runner and the intersection between of shroud and trailing edge of the blade. [9]

It can be obtained as in expression below:

$$R_{2e} = \left(\frac{Q/\pi\omega}{\phi_{2e}}\right)^{\frac{1}{3}} \tag{3.2}$$

where ϕ_{2e} is the flow coefficient and is a function of specific rotational speed. It can be obtained from a graph having a plot of specific rotational speed versus flow coefficient.

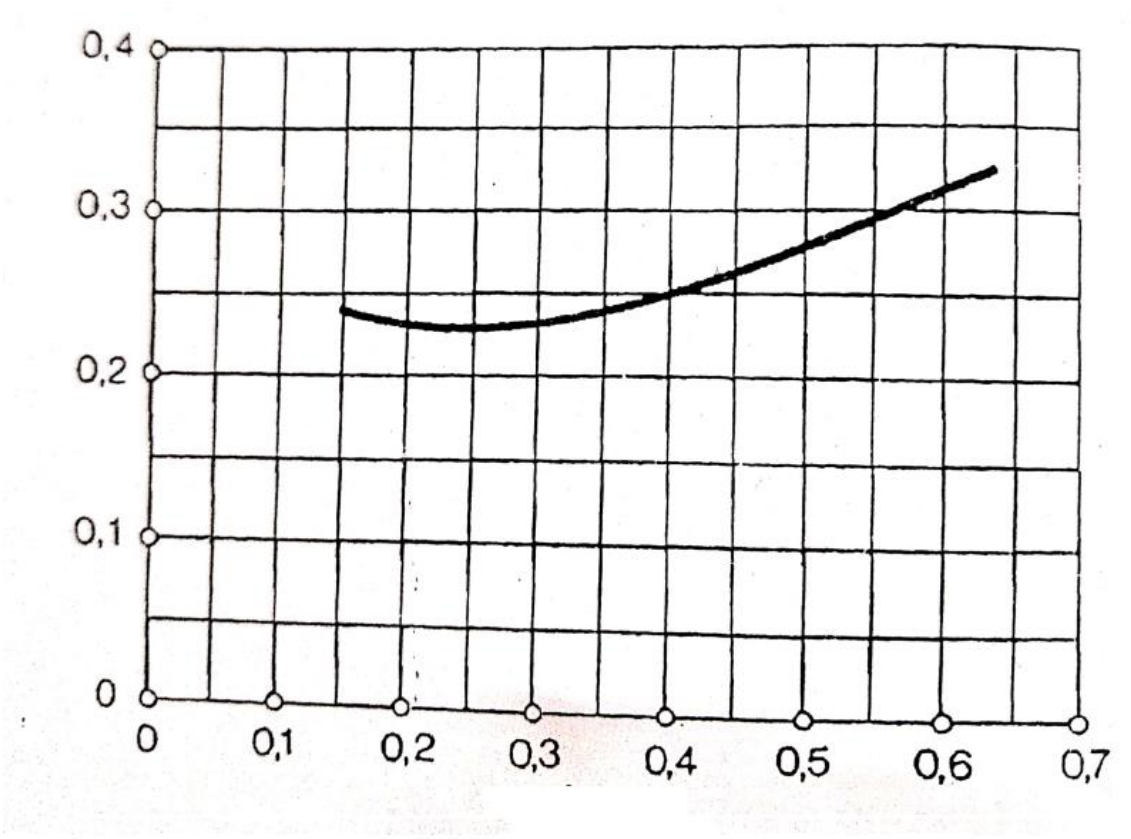

Figure 3.2 Graph of Specific rotational speed vs Flow coefficient [9]

R_{li} is the distance between the rotational axis and the intersection of the hub and leading edge of the blade which can be obtained by the expression below:

$$R_{li} = \left(\frac{2gH}{(\psi_{li})^{\omega^2}}\right)^{\frac{1}{2}} \tag{3.1}$$

where, ψ_{li} is the specific energy coefficient which is also a function of specific rotational specific speed and is obtained from the graph below [9]:

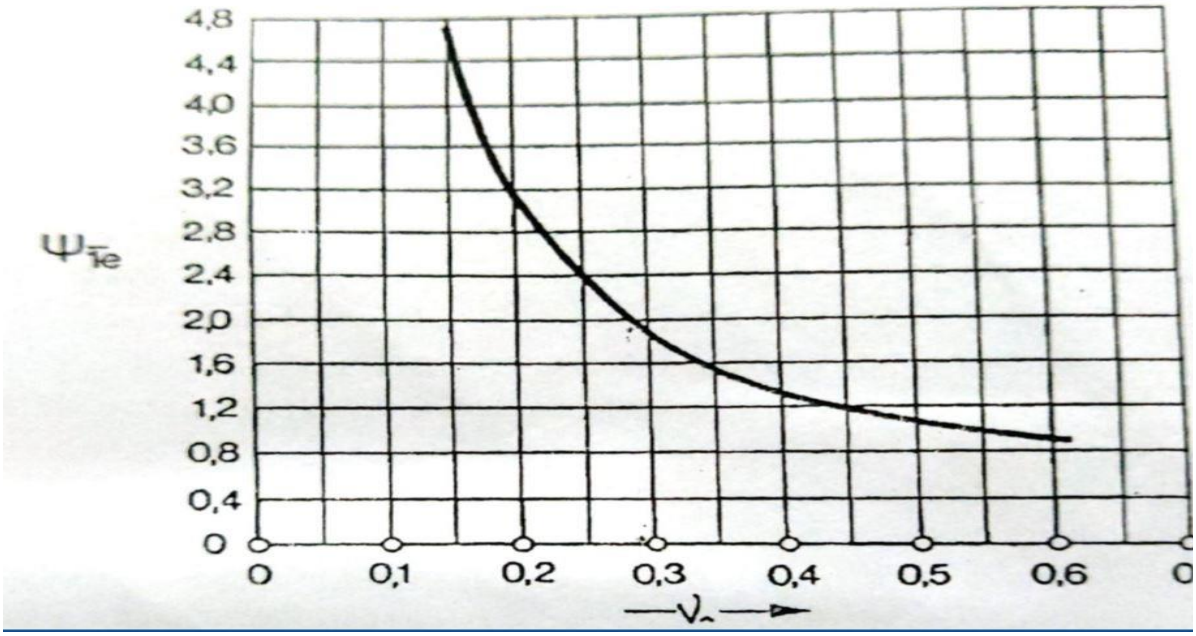

Figure 3.3 Graph of Specific rotational speed vs Energy coefficient[9]

After the limiting point of the meridional view is obtained other parameters shown in the above figure can be obtained from the equations mentioned below.

$$r_{li} = \frac{R_{li}}{R_{2e}} = \frac{\phi_{2e}^{\frac{1}{3}}}{\psi_{li}^{\frac{1}{2}}} - \frac{1}{n_0^{*\frac{2}{3}}} \tag{3.2}$$

$$b_0 = \frac{B_0}{R_{2e}} = 0.8(2 - n_0^*)n_0^* \tag{3.3}$$

$$r_{oi} = \frac{R_{oi}}{R_{2e}} = 0.7 + \frac{0.16}{n_0^* + 0.08} \tag{3.4}$$

$$l_{1i} = 3.2 + 3.2(2 - n_0^*)n_0^* \tag{3.5}$$

$$l_{1i} = 0.8 + b_0 \tag{3.6}$$

$$l_e = 2.4 - 1.9(2 - n_0^*)n_0^* \tag{3.7}$$

$$r_{oe} = r_{1i} = \frac{0.493}{(n_0^*)^{\frac{2}{3}}} \qquad n_0^* \leq 0.275 \;\; ; \;\; n_s \leq 160 \tag{3.8}$$

$$r_{oe} = 1.255 - 0.3n_0^* \qquad n_0^* > 275 \;\; ; \;\; n_s > 160 \tag{3.9}$$

The relation between the specific rotational speed and the meridional channel parameters are not linear as seen above. This kind of relations causes the variation in different type of blades according to the specific rotational speed. The curves defining the outlet of the meridional plane using equation of crown and hub and values of y_{me}, y_{mi}, y_{2e} & x_{2e}.

By Bovet,

$$y_{me} = \frac{y_{2e}}{\frac{y_{2e}}{y_{me}}} = \frac{r_{oe} - 1}{\frac{y_{2e}}{y_{me}}} \tag{3.10}$$

$$r_{me} = r_{oe} - y_{me} \tag{3.11}$$

$$y_{mi} = r_{oi} \tag{3.12}$$

From equation,

$$\frac{y}{y_m} = 3.08\left(1 - \frac{x}{l}\right)\sqrt{\frac{x}{l}\left(1 - \frac{x}{l}\right)} \tag{3.13}$$

Values lead to the actual dimensions of the runner by multiplying dimensionless quantity R_{2e}.

$$\left[\frac{Y}{Y_m}\right]_{i,e} = \left[3.08\left(1 - \frac{X}{L}\right)\sqrt{\frac{X}{L}\left(1 - \frac{X}{L}\right)}\right]_{i,e} \tag{3.14}$$

Putting respective values of i & e gives the hub and shroud curve respectively. The hub curve is a quarter parabola and the shroud curve is a complete parabola.

Obtain the table in which

$$X_{i,e} = x_{i,e}\, R_{2e}$$
$$Y_{i,e} = y_{i,e}\, R_{2e} \qquad (3.15)$$
$$L_{i,e} = l_{i,e}\, R_{2e}$$

Table 3.1 Meridional Parameters

x_i	x_e	y_e	y_i	X_i mm	X_e mm	Y_i mm	Y_e mm	Obs

where, $x_i = [\ 0\ ,\ l_i/4\ ]$ & $x_e = [\ 0\ ,\ l_e\ ]$

The parameters in the lower case are dimensionless specific values and the parameters in upper case are the real values.

3.2 Runner Blades

Axial View of the runner

After fixing the limit points of the meridional channel the leading edge and trailing edge of the blades is fixed. Leading edge and trailing edge are parabolas having its center of rotation at the shroud points and passing through the limiting points in the hub curve.

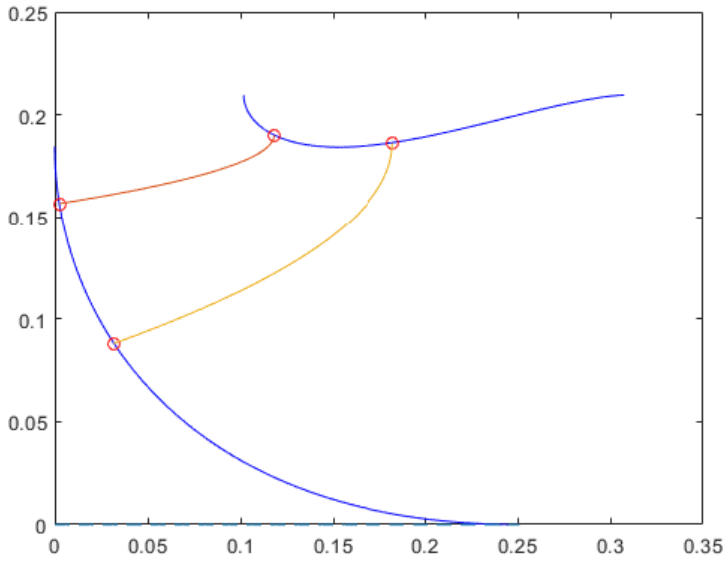

Figure 3.4 Meridional View with limiting points leading and trailing edge marked by circles at hub and shroud respectively

Inserting streamlines in through the flow channel

The streamlines are inserted by interpolating the curves of hub and shroud. The equations of streamlines must be similar to the hub curve and shroud curve i.e. must be a part of parabola.

The number of streamlines can be chosen any number as per the designer's choice.

For interpolating the streamlines

Change in length of streamline from the hub curve to the shroud curve is obtained as:

$$dlstream = \frac{(L_i - L_e)}{number\ of\ streamlines + 1} \tag{3.18}$$

Change in maximum value for each streamlines from the hub to shroud curve is obtained as:

$$dyms = \frac{(Y_i - Y_{me})}{number\ of\ streamlines + 1} \tag{3.19}$$

Change in starting point for each streamlines along the x-direction / guide vane height factor is expressed as:

$$bfactor = \frac{B}{number\ of\ streamlines + 1} \tag{3.20}$$

Also as shroud is a complete parabola and hub is a quarter parabola so the change in length factor for streamlines is expressed as:

$$dlfactor = \frac{\left(1 - {}^{1}/_{4}\right)}{number\ of\ streamlines + 1} \tag{3.21}$$

Length of streamline starting from the shroud curve can be expressed as:

$$Lstream = L_e + dlstream \tag{3.22}$$

Shift of streamline from the shroud curve is expresses as:

$$Bstream = bfactor * (number\ of\ streamlines + 1) \tag{3.23}$$

Now the equation of streamlines can be expressed as in terms of these interpolated parameters as

X component of the streamlines is length of streamlines multiplied by the change in length factor

$$Xstream = lstream * dlfactor \tag{3.24}$$

Y component of the streamlines can now be obtained by plotting these interpolated elements in the previously given parabolic equations of hub and shroud as:

$$\left[\frac{Y}{Y_{me}+dyms}\right]_{stream} = \left[3.08\left(1-\frac{Xstream}{Lstream}\right)\sqrt{\frac{Xstream}{Lstream}\left(1-\frac{Xstream}{Lstream}\right)}\right]_{stream} \quad (3.25)$$

The above equation gives the equation of streamlines starting from the hub curve and needs to be shifted along the guide vane height and needs to be plotted as:

$$Xstreamlines\ plot\ = Xstream + bstream \quad (3.26)$$

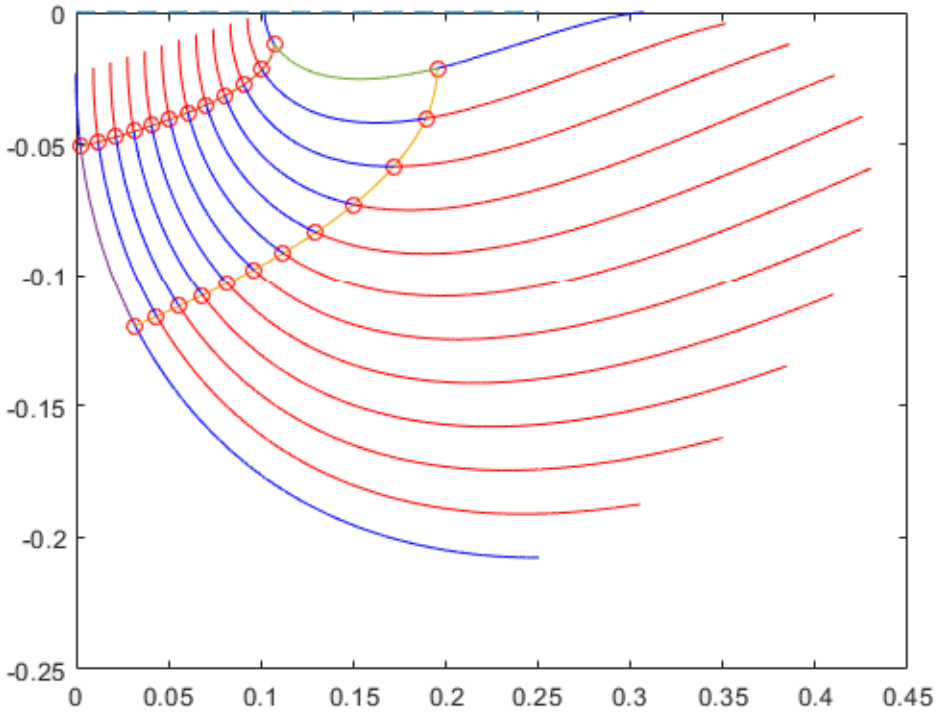

Figure 3.5 Meridional View with streamlines

After obtaining the streamlines, it needs to be considered only from the leading to the trailing edge and is converted into equal number of points from the leading to the trailing edge in every streamline as shown below.

The streamlines from leading to trailing edge can be converted into any number of equal divisions.

The point of intersection of streamlines and the leading edge are the starting points and the points of intersection between the trailing edge and streamlines are the end points.

Change in x component of streamlines can now be expressed as

$$dxstream = \frac{Xstream\ start - Xstream\ end}{number\ of\ divisions} \tag{3.27}$$

Plotting above equations for obtaining equal number of divisions from leading to trailing edge as:

The equation for these streamlines can be expressed as:

$$\left[\frac{Yplotstream}{Y_{me} + dyms}\right]_{stream} = \left[3.08\left(1 - \frac{Xplotstream}{Lstream}\right)\sqrt{\frac{Xplotstream}{Lstream}\left(1 - \frac{Xplotstream}{Lstream}\right)}\right]_{stream}$$

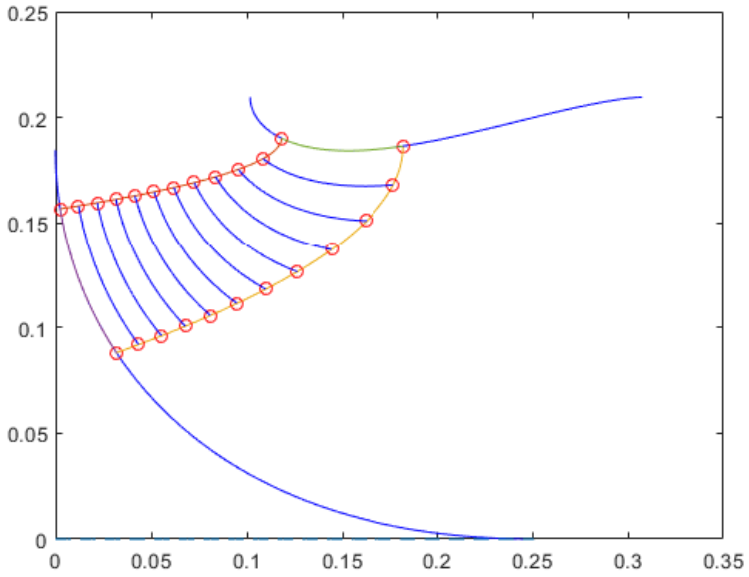

Figure 3.6 Meridional View with streamlines in blade only

Beta Distribution in the blade

The beta angle is determined by the equations mentioned below[10]:

$$cot\beta_1 = \frac{\pi D_1 B}{Q}\left(\frac{\pi D_1^* N}{60} - \frac{60gH}{\pi D_1^* N}\right) \tag{3.29}$$

where,

β_1 is the angle at the leading edge

D_1 is the maximum diameter at inlet

D_1^* is changing diameters of inlet from the shroud to hub along the leading edge

$$tan\beta_2 = \frac{{}^{Q}/_{A_2}}{\frac{\pi D_2^* N}{60}} \quad (3.30)$$

where,

A_2 is the area at the outlet of the runner obtained as $A_2 = \pi * D_2^2 / 4$

D_2^* is changing diameters of outlet from shroud to hub along the trailing edge.

After finding beta angles at the inlet and outlet of the blades, the beta distribution along the streamline is chosen to be linear from the leading to the trailing edge and this plot can be seen as in figure below:

Beta distribution has been chosen to be linear for simplicity in the design of the profile of the blade however, it can also be chosen elsewise.

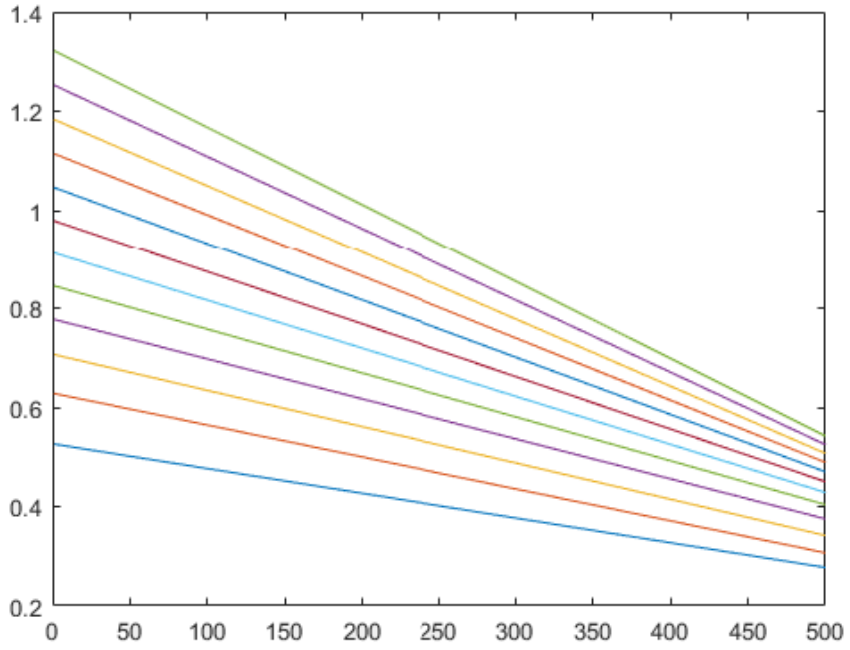

Figure 3.7 Beta Distribution along leading to trailing edge

Determining the energy distribution in the blades (U-C_u)

The beta distribution gives Cu component of every point through the streamline by constructing a velocity triangle. U component is a function of diameter and rotational speed of the blades. The plot of U-Cu distribution should be smooth.

$$U = \frac{\pi DN}{60} \quad (3.31)$$

Where, D is the diameter at the required point

N is the rotational speed of the runner

Cm component at the inlet is obtained by the expression as:

$$C_{m1} = \frac{Q}{\pi D_1 B} \tag{3.32}$$

At the outlet is given by the expression

$$C_{m2} = \frac{Q}{\pi D_2^2} \tag{3.33}$$

The Cu component is obtained as:

$$C_u = U - \frac{C_m}{tan\beta} \tag{3.34}$$

U-Cu distribution gives the shape of the blade along the streamlines; thickness of the blade is determined by the energy conversion in the blades. It is generally desirable to have more energy conversion in the beginning of the blades. Blades are thinner at the outlet due to less tension. The slip angle should not be large as it may cause cavitation due to the difference in the pressure at the pressure and the suction side. The Cu component should not be larger than the U component at the same point.

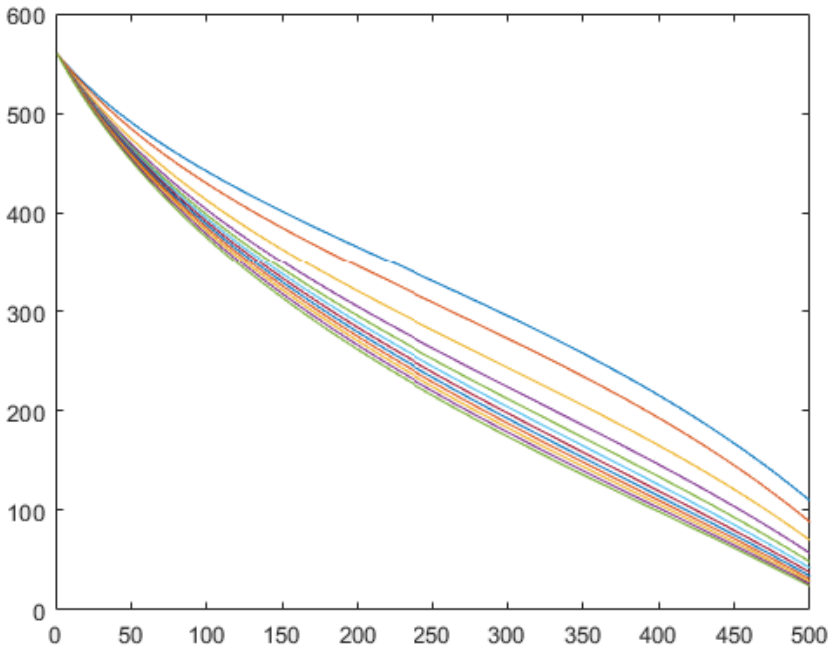

Figure 3.9 U-Cu Distribution from inlet to outlet

The figure above shows that the energy conversion in the streamlines is almost equal however some differences can be seen due to the varying profile and results in varying thickness of the blade.

Theta Distribution in the blades

To plot the radial view of the blades theta angles of the blade is determined. This is done by determining a new plane G-H plane which simplifies the conversion of axial plane into radial plane. A G-H plane is a plane formed along the length of the streamlines in the blade. The G and H are defined as:

G – Length of streamline in the axial plane.

H- Length of streamline in the radial plane.

Length of streamline in the axial plane (G) is obtained by integrating the distances of consecutive points in the streamlines of the axial plane plotted before. This is done by converting the axial co-ordinates x&y to R&Z.

R & Z is defined as

R is the radius of any point from the axis of rotation

Z is the horizontal distance of any point along the axis of rotation.

After that the change in length along the G plane is obtained as:

$$dg_{1,i} = \sqrt{(R_{2,i} - R_{1,i})^2 + (Z_{2,i} - Z_{1,i})^2} \tag{3.35}$$

Change in length of streamline along the radial plane is known by knowing the change in length along the axial plane and beta distribution as:

$$dH_{1,i} = \frac{dg_{1,i}}{tan\beta} \tag{3.36}$$

Knowing these change of length along the streamline in axial and radial plane theta angle can be determined. Starting point for the calculation is taken as:

$R_{start} = \frac{D_1}{2}$ & θ = 0

The theta angle is given as[4]:

$$\mathrm{d}\theta = \frac{\Delta H}{R} \tag{3.37}$$

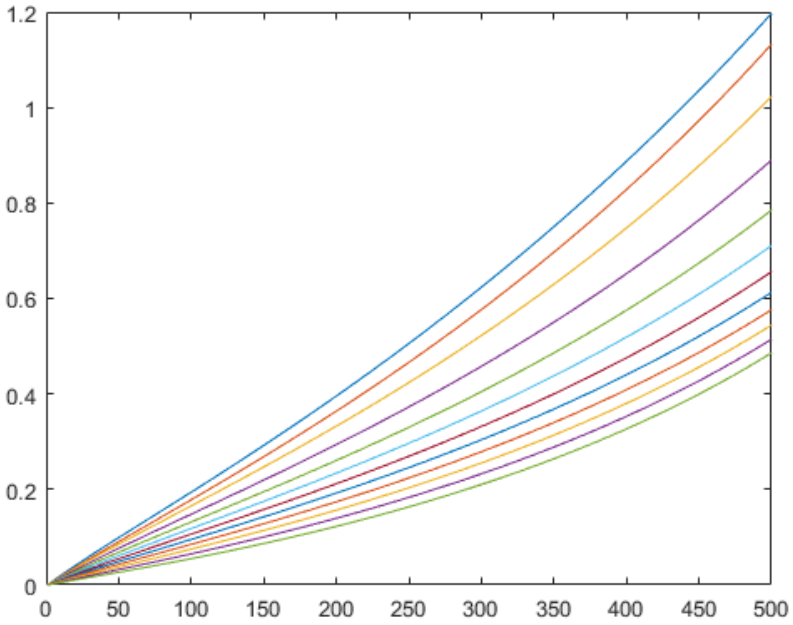

Figure 3.10 Theta Distribution from inlet to outlet

The Y-axis is in radians and the X-axis is in millimetres. Theta angle increases from the leading to the trailing edge and it shows that the relation in somehow logarithmic.

Radial View of the blades

The radial view is obtained by plotting the radius and theta angle throughout the blades.

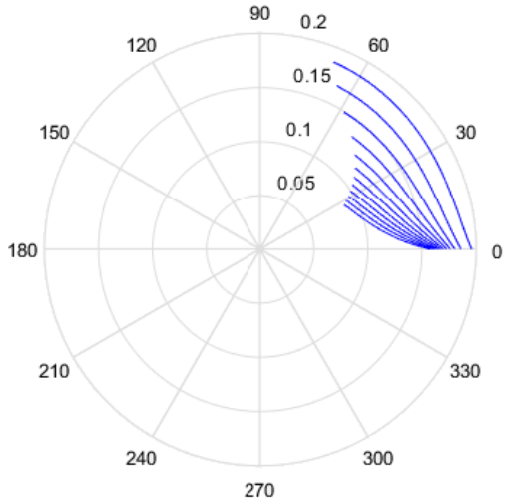

Figure 3.11 Radial View of blade streamlines

The radial view is a polar plot representing the angles and the length of streamlines along the blades. It can be seen that the streamlines are less curved for the shroud curve and more curved for the hub profile. The angular variation in the plot is the theta angle variation obtained in the previous section.

3D view of the blade

The combination of axial view and the radial view gives the 3D view of the blade. R and theta is obtained from the radial view whereas Z component is obtained from the axial view. Plotting these

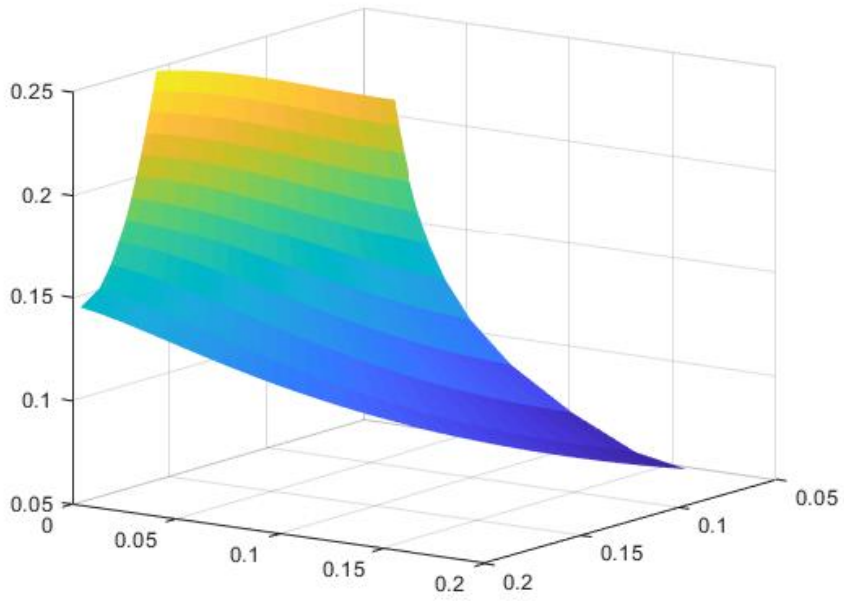

Figure 3.12 3D view of single blade (suction side)

The 3D view of the blade in the figure shows the leading edge at the left and the trailing edge at the right side. The plot has been generated in the design software with all the coordinates obtained from previous calculations.

3D of Hub and shroud

The hub curve and the shroud curves are revolved along the rotational axis having the thickness calculated from mechanical design.

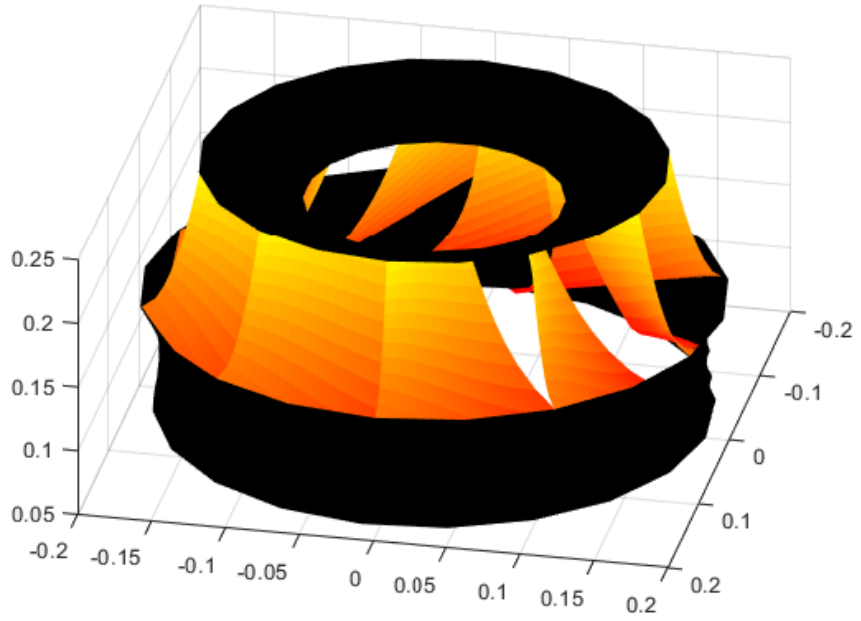

Figure 3.13 Runner assembly

3D of single blade obtained in the previous section is rotated along the rotational axis to obtain the blade configurations. The hub and the shroud are according to the profile of the hub and shroud curve respectively. However, the length of the hub curve can be extended up to the rotational axis not only up to the blade profile.

Design of Guide Vanes

Guide vanes are designed to direct controlled flow of water towards the runner blade allowing control in hydraulic input power. Flow required and pressure conditions of runner are major design criteria of guide vanes[11].

There is no energy loss in the flow from guide vane outlet to the runner inlet as there is a change in velocity energy and pressure energy only. A free vortex theory can be used as shown in equation (3.38)

$$Cu_1 R_1 = Cu_{gvo} R_{gvo} \tag{3.38}$$

Cu is the tangential component of absolute velocity. The meridional component of absolute velocity is given by equation (3.39).

$$Cm_{gvo} = \frac{Q}{2\pi \cdot B_{gv} . R_{gvo}} \quad [\text{m/s}] \tag{3.39}$$

The outlet angle of guide vane will be same as angle between the tangential and absolute velocities from inlet velocity triangle which can be expressed as shown in equation (3.40).

$$\alpha_1 = tan^{-1}\frac{Cm_1}{Cu_1} \tag{3.40}$$

However, the outlet angle of guide vane needs some correction due to small cross section area at outlet. There are various methods for designing guide vanes. Better direction of flow is given by longer guide vanes. However, frictional loss is more in longer guide vanes. Operational requirement determine the shape of guide vanes. The shape affects the distribution of velocity and pressure. Generally, the NACA airfoils are good choice for guide vanes shape. Guide vane axis diameter is important for guide vanes for proper control if guide vane apparatus servo or chain link does not work properly. During operation a net rotating torque is experienced so that proper design should be done to ensure timely closure and proper positioning of guide vanes.

Diameter of guide vane outlet should be five percent larger than the diameter of runner inlet which is a starting point for guide vane dimensions. The location of guide vane axis diameter is expressed as in equation (3.41)[4]

$$D_{ax} = D_1(0.29 \cdot \Omega + 1.07) \qquad [m] \tag{3.41}$$

D_1 is the diameter of runner inlet and **Ω** is speed number. Minimum length of guide vane is found by using axis diameter and number of guide vanes in order to stop the flow. In order to prevent the guide vanes to rotate full circle guide vanes have to overlap. Generally, 10-20% overlap factor is chosen. Length of guide vane is expressed as in equation (3.42).

$$L_{gv} = \frac{\pi \cdot D_{ax} \cdot k_{cf}}{N_{gv}} \qquad [m] \tag{3.42}$$

L_{gv} is the length of guide vane, k_{cf} is the coverage factor and N_{gv} is the number of guide vanes. The diameter of guide vane inlet is calculated by using cosine theorem as expressed in equation (3.43).

$$D_{gvi} = \frac{\sqrt{L_{gv}^2 + (\frac{D_{gvo}}{2})^2 - 2 \times L_{gv} \times \left(\frac{D_{gvo}}{2}\right) \times \cos\left(\frac{\pi}{2} - \alpha_0\right)}}{1/2} \qquad [m] \tag{3.43}$$

Guide vane axis diameter should be checked and recalculated using cosine theorem if guide vane axis is too close to guide vane outlet. Generally, axis should be located at 2/3 of guide vane length from outlet. The coverage factor is also then changed.

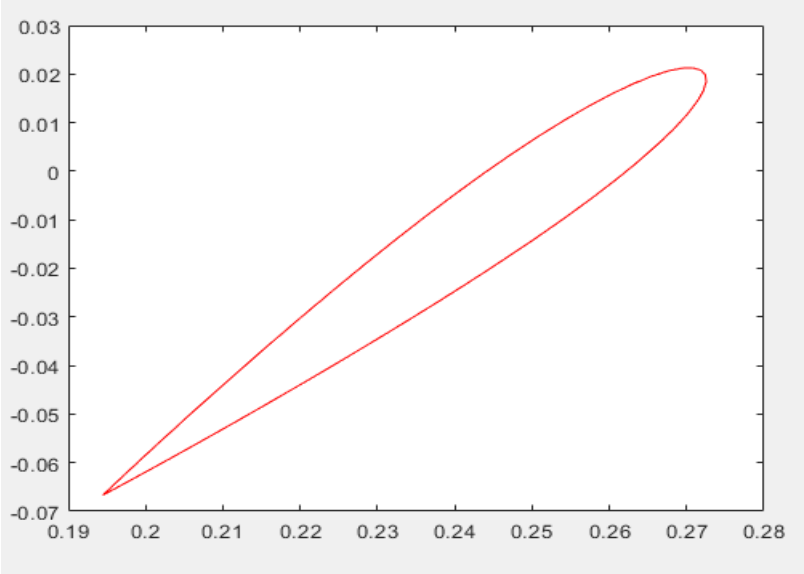

Figure 3.14 Single Guide Vane

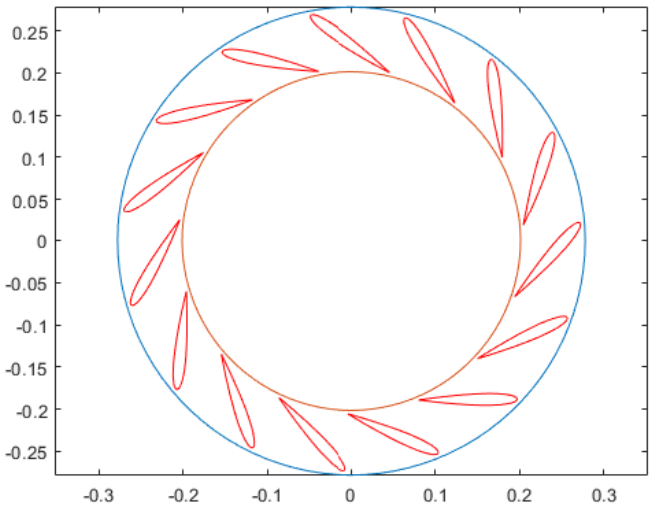

Figure 3.15 Guide Vane Assembly

Design of Stay vanes

Stay vanes are designed to withhold forces from the pressure acting on spiral casing and have no hydraulic effect. For simplicity, the area in which pressure acts can be assumed an annulus with constant inner and outer diameter as of inlet spiral case. At full load condition diameter of stay vane outlet is 2% greater than guide vane inlet diameter. The gap can vary between 1-

5%.Free vortex assumption is made in the flow through the gap, flow through stay vane and throughout spiral case as expressed in equation (3.44).

$$Cu_{gvi} \cdot R_{gvi} = Cu_{svo} \cdot R_{svo} = constant \tag{3.44}$$

Determination of optimal length of a stay vane is an iterative process. Initially diameter of stay vane inlet is chosen. Minimum length of stay vane is expressed as in equation (3.45).

$$L_{sv} = \frac{F_{max}}{\sigma_{steel} \cdot t_{sv} \cdot Z_{sv}} \quad [m] \tag{3.45}$$

F_{max} is the maximum force due to water head on the spiral casing, σ_{steel} is the strain property of the material, Z_{sv} is the number of stay vanes, t_{sv} is the thickness of stay vane. For BEP equal number of guide vanes and stay vanes should be chosen. Thick stay vanes will disturb the flow pattern and decrease in flow area. These two concerns should be a compromise.

D_{svi} is obtained forming stay vane as free vortex streamline. New D_{svi} is used to calculate new spiral case that gives new area of annulus for next iteration step. The leading edge and trailing edge of stay vane should be designed to disturb the flow minimally. As stay vanes have thickness flow area decreases so that in order to compensate the trailing edge angle should be chosen to be 30degrees.Leading edge can be defined as a half circle. Minimum thickness for stay vane is about 2mm.

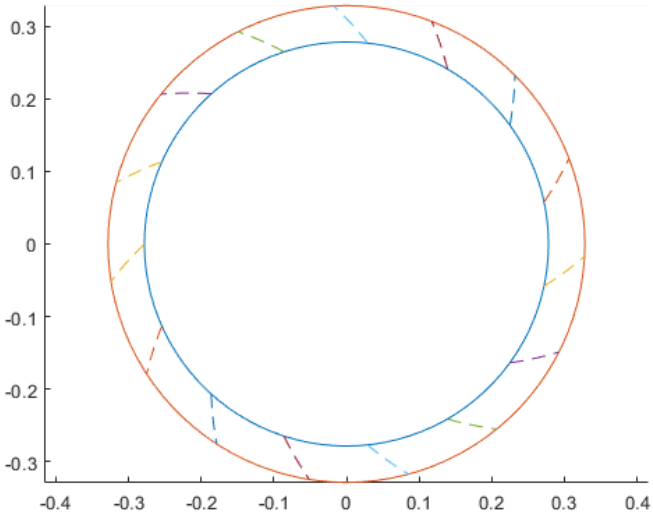

Figure 3.16 Stay Vane Assembly

Design of casings

Uniform distribution of flow in runner is achieved only when flow is uniform in vanes. Spiral casing provide uniform flow in vanes. The design of casing is dependent on the flow and pressure condition of runner as listed in Table 1. A certain circulation must be formed for proper incidence angle of water around the vane. Among accelerated, deceleration and free vortex type of spiral casing free vortex is chosen for simplicity, in which the design is based on the law of constant velocity moment,

$C_u.R = C_t = \text{constant}$ (3.46)

The outlet tangential velocity is taken as equal to the inlet tangential velocity of the vane. Required inlet flow condition of spiral casing is chosen so as to match the outlet tangential velocity using an iterative process. The inlet flow is transformed to an inward radial (C_m) and tangential/peripheral (C_u) flow. Tangential flow is responsible for generation of required circulation for proper reaction ratio for runner.

Circular Cross Section

Flow in each section of spiral casing is determined from the fact that constant water flow must be provided from spiral casing. Dimensions of all the section is calculated using iterative process. The radius of each section 'r' is determined with the help of circulation 'C_t'. To ensure exact circulation strength, the iteration is carried out until there is match between required vortex at inlet of vane and computed vortex at spiral casing.[6]

$$C_t = \frac{Q}{2 \cdot r^2 \int_{\varphi_0}^{\pi} \left(\frac{sin^2 \varphi}{R_T - r \cdot cos\varphi} \right) d\varphi} \quad (3.47)$$

$$C_u = \frac{Q}{R \cdot 2 \cdot r^2 \int_{\varphi_0}^{\pi} \left(\frac{sin^2 \varphi}{R_T - r \cdot cos\varphi} \right) d\varphi} \quad (3.48)$$

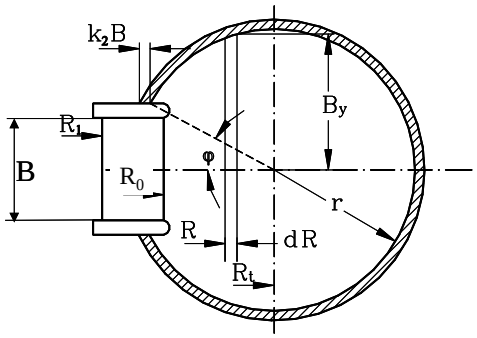

Figure 3.17 Circular cross section of spiral

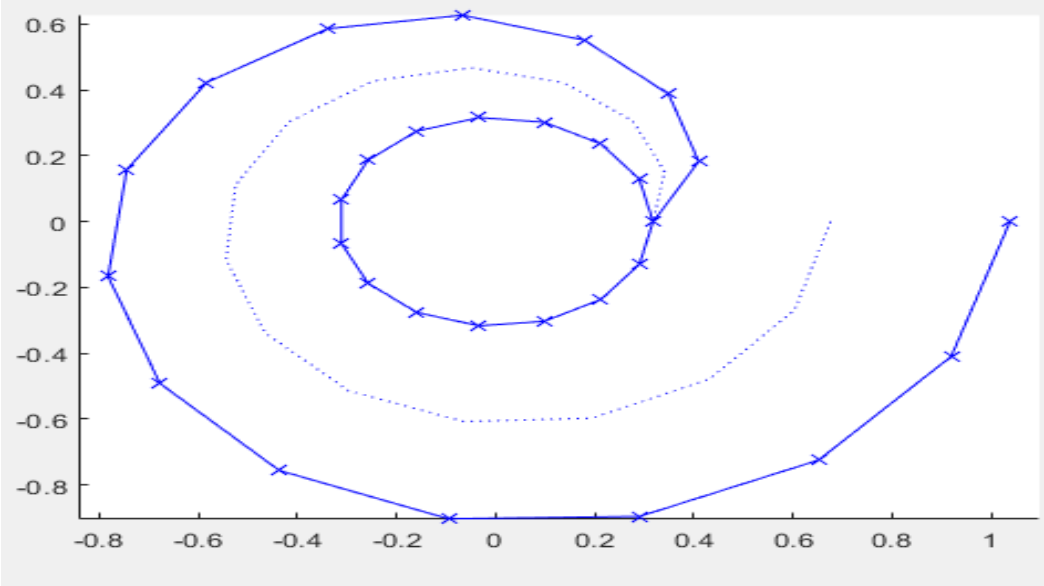

Figure 3.18 Spiral Case plot with outer, mid and inner curve

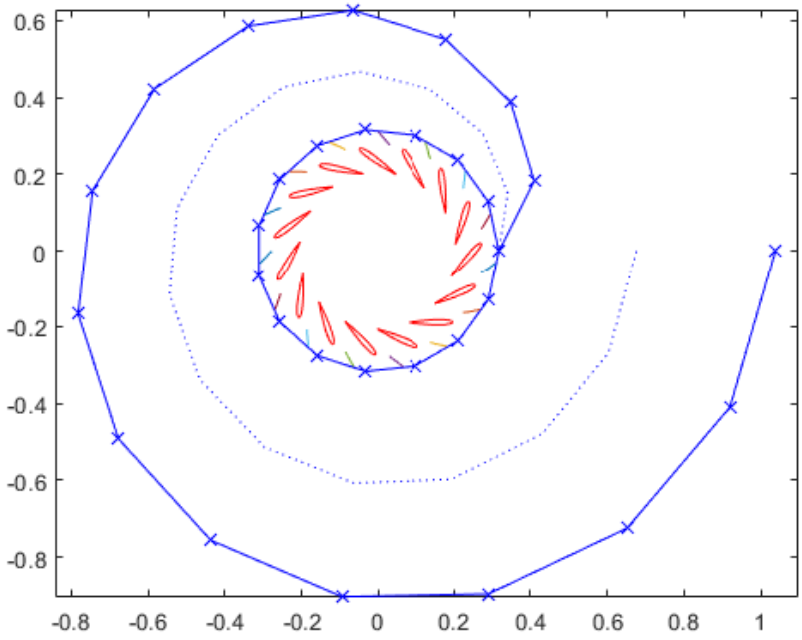

Figure 3.19 Casing and Vanes plot

CHAPTER 4 EXPERIMENTAL PROCEDURES AND RESULTS AND COMPARISON WITH NUMERICAL RESULT

4.1 Turbine Testing Procedures

Turbines are designed to obtain certain output and perform accordingly in the operating conditions. So, turbine designed and developed needs to be checked either in the laboratory or at the site to obtain the performance and operating characteristics of the turbine. In case of small hydro turbines the testing can be done in the site or at laboratory. However, larger turbines need to be scaled down and tested in the laboratory before actual operation in the site. The laboratories test help to find out the efficiency, runaway speed, performance characteristics, etc. of the turbine.

Experiments have been conducted in a test set-up in the Turbine Testing Laboratory of KU shown as in Figure 4.1.

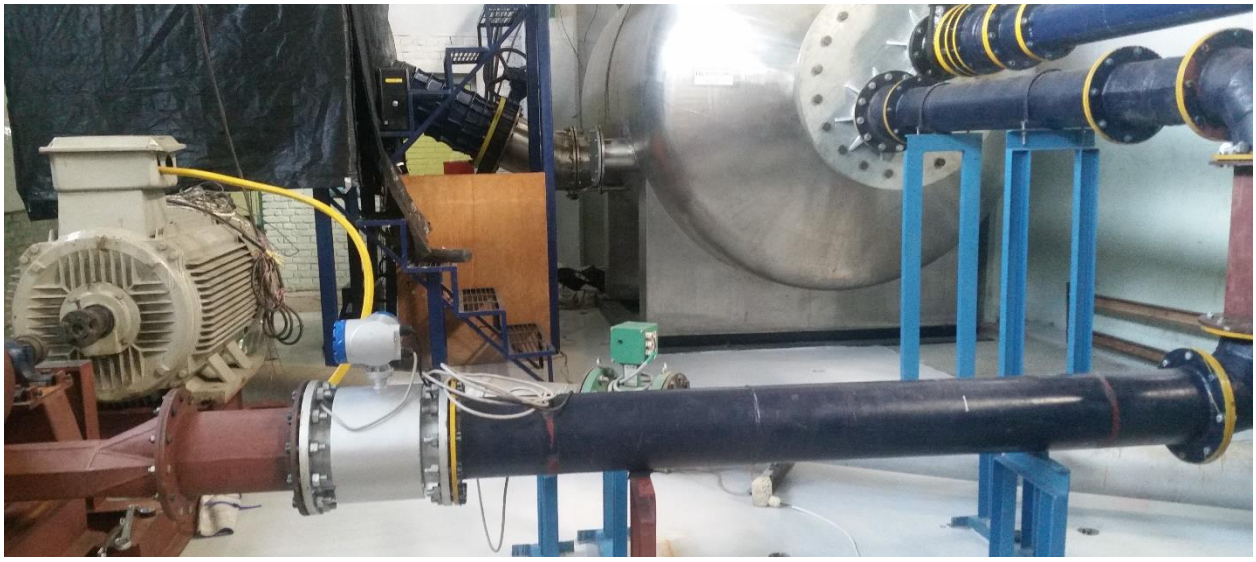

Figure 4.1 Lab Setup of Test Rig

The experimental rig was fabricated at Thapa Engineering Pvt. Ltd, Butwal and assembled under technical supervision at TTL, KU. Turbine inlet is connected to the available system loop from the high pressure tank and the outlet of the turbine is allowed to pass to the sump freely beneath it. A pump is connected to provide the required flow and head to the turbine. Electromagnetic flow meter is connected at the inlet at a distance of five times the outlet diameter of the runner. Two pressure sensors are connected. One at an inlet of the spiral casing and one at the outlet of the runner i.e., in the draft tube. The turbine is coupled with an induction motor through a torque transducer. The induction motor acts as the load in the testing process.

The speed of the turbine is varied through a VFD connected to the motor. The obtained data was logged using an in-built program in the data logger. Experiments were carried out at different speeds and variable flow. The technical specifications along with the purpose of the equipment used have been listed in the table below:

Table 4.1 Equipment used with their specifications

S.N.	Equipment	Specifications		Purpose
1.	Pump	Head : up to 75m Power: 250 HP		Water supply to test rig
2.	Flow meter	Type: Electromagnetic Model: KTM-800 Output: 4-20 mA DC		Flow measurement
3.	Pressure Sensor	Inlet Type: APC-2000ALW Pressure: 0-2.5 MPA Abs T_{amb}: -40 - +85^o C	Outlet APC-2000 ALW 0-700 kPa -40 - +85^o C	Head Measurement
4.	Torque Transducer	Model: YDRM – 50KM Capacity: 50 kgf-m		Torque measurement
5.	Induction Motor	Type: 3 Phase Model: YJTG355M-2 Power: 250 kW Inlet: 5-100 Hz		Loading Device
6.	VFD	Model: ZVF300-G250/P280T4M Power: 250/280 kW Input: 3PH 50/60 Hz Output: 3PH 0-600 Hz		Variable speed drive
7.	Precision Digital Indicator	Model: YD-3533-AZ & YD-7532 Power: 220 AC Excitation: 12 V Input: mV/V & rpm Output: 10V & 0-10V		Data logging

While starting the experiment, VFD was started to control the rpm of the induction motor. Then, the pump is started by increasing its rpm until the level of water reaches a certain height

in the high pressure tank which is seen by the indication marked on the pipe extending from the high pressure tank. This helps to maintain required pressure in the turbine. The by-pass valve in the high pressure tank allows to control the flow through the turbine. The required parameters were recorded in the data logger and the data obtained were used for performance analysis.

Efficiency of the turbine is calculated as:

$$\eta = Power\ output/power\ input = \frac{\tau * \omega}{\rho * Q * g * H} \quad (5.1)$$

For both the casted and forged runner the experimental procedures were similar and the performance curves were obtained.

4.1.1 Results and discussions

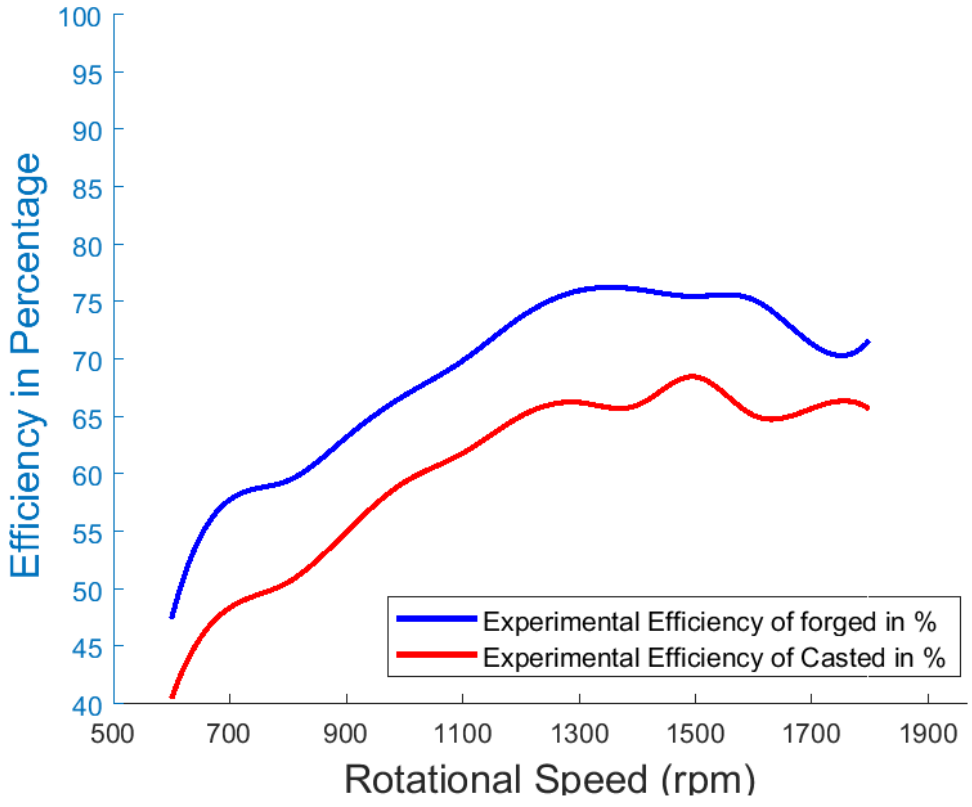

Figure 4.2 Experimental Efficiency of Casted and Forged Runner

Figure 4.2 shows the efficiency of the turbine with the variation in rotational speed of the rotor. Rotational speed of the motor was varied from 600 to 1800 rpm. The highest efficiency was obtained as 68% at 1500 and 76% at 1400 rpm for casted and forged runner respectively. The curves depicts an increase in efficiency up to the design rpm and decrease later The decrease in efficiency at higher rpm may be accounted due to the vibration in the set-up and heating

problem in the bearing hub. At the designed rpm of the turbine .i.e. 1500 rpm, 14kW power was generated with an efficiency of 75 %.

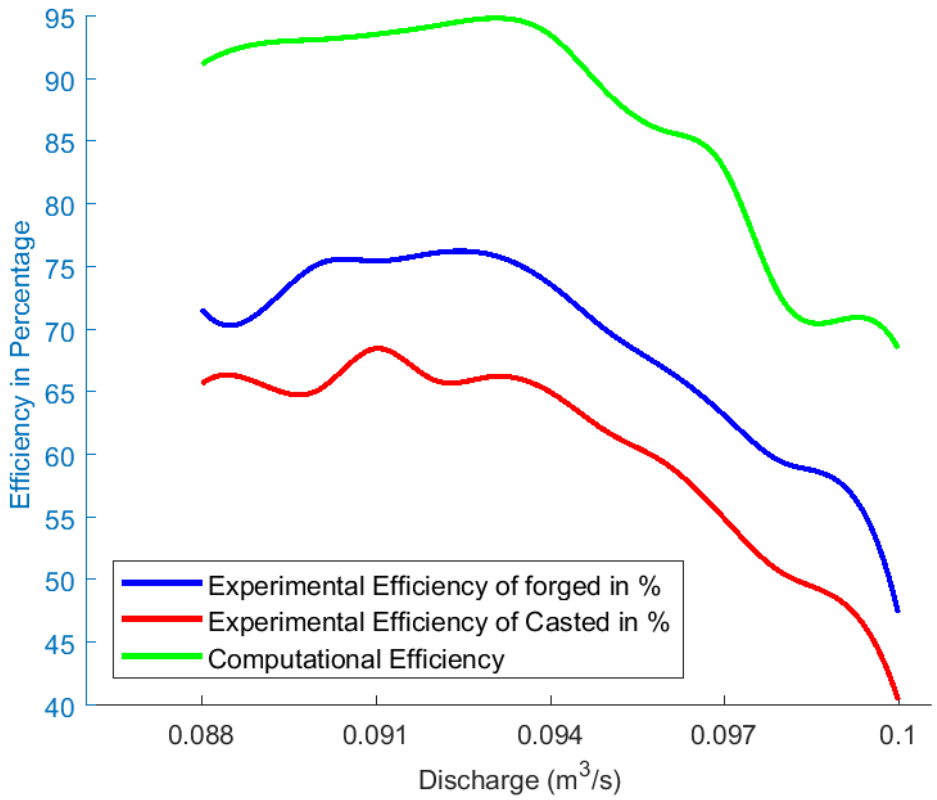

Figure 4.3 Experimental Efficiency of Casted and Forged Runner at Varying Discharges

Figure 4.3 shows the efficiency of the turbine with the variation in the flow rate. The flow rate was varied from 0.085 m^3/s to 0.1 m^3/s which was controlled by varying the rpm of the pump as well at different opening of bypass valves present in the high pressure tank. The performance curves in Fig 5.3 shows similar tends of efficiency curves for both the runners. The highest efficiency is obtained at around 0.091 m^3/s and 0.093 m^3/s for casted and forged runners respectively. The limitations in this experiment was due to the lack of inlet valve to accurately control the varying flow also the VFD rejected certain flows.

The efficiency of the forged turbine was found to be better due to the manufacturing accuracy. The casted runner contained holes and also the leading and trailing edge profile was not accurately manufactured as designed. These manufacturing defects may have caused the decrease in power output as well as efficiency.

CHAPTER 5 NUMERICAL PROCEDURES AND RESULTS

5.1 Numerical Modeling

Computational Fluid Dynamics is a tool to analyze and solve problems that involve fluid flows. It incorporates the solution of the fundamental equation of fluid flow, the Reynolds- averaged Navier Stokes equations, using turbulence models to compute the averaged turbulence stresses. The Navier-Stokes equations represent the laws of conservation of mass, momentum and energy in differential form. These partial differential equations in integral form are then approximated as finite-volume expressions and reformed into algebraic equations to allow for numerical computation within a specified domain.

ANSYS CFX solves the unsteady Navier-Stokes equations in their conservative form. The instantaneous equation of mass (continuity) in the stationary frame is expressed as equation (5.1)

$$\frac{\partial \rho}{\delta t} + \nabla \cdot (\rho U) = 0 \tag{5.1}$$

And the instantaneous equation for the momentum is expressed as shown in equation (5.2)

$$\frac{\partial \rho}{\delta t} + \nabla \cdot (\rho U \otimes U) = -\nabla \mathrm{p} + \nabla \cdot \tau + S_M \tag{5.2}$$

where τ is the stress factor,

These instantaneous equations are averaged for turbulent flows leading to additional terms that need to be solved. While the Navier-Stokes equations describe both laminar and turbulent flows without addition terms, realistic flows involve length scales much smaller than the smallest finite volume mesh. Therefore, much research has to be done to predict the effects of turbulence by using turbulence models. These models account for the effects of turbulence without the use of a very fine mesh or direct numerical simulation. These turbulence models modify the transport equations by adding averaged and fluctuating components.

The transport equations are changed to equations (5.3) and (5.4):

$$\frac{\partial \rho}{\delta t} + \nabla \cdot (\rho U) = 0 \tag{5.3}$$

$$\frac{\partial \rho U}{\partial t} + \nabla \cdot (\rho U \otimes U) = -\nabla \mathrm{p} + \nabla \cdot \{\tau - \rho u \otimes u\} + S_M \tag{5.4}$$

The mass equation is not changed but the momentum equation contains extra terms which are the Reynolds stresses, ρu⊗u and the Reynolds flux, ρuØ. These Reynolds stresses need to be

modeled by additional equations to obtain closure. Obtaining closure implies that there are a sufficient number of equations to solve for all the unknowns including the Reynolds stresses and Reynolds fluxes.

Various turbulence models provide various ways to obtain closure. In this investigation, Shear Stress Transport (SST) model was utilized. The advantage of using this model is that combines the advantages of other turbulence models (the k-Є, Wilcox k-ω and BSL k-ω). In order to understand the advantage the SST model, 3 other models will be discussed briefly.

5.1.1 Turbulence models

Two-equation turbulence models are widely used in CFD as they give a good compromise between computational power needed and accuracy. The term 'two equation' refers to the fact that these models solve for the velocity and length scales using separate transport equation. The turbulent length scale is estimated from two properties of the turbulence field, namely the turbulent kinetic energy and the dissipation rate. The dissipation rate of the kinetic energy is obtained from its transport equation. The most widely used are k-Є and k-w two equation models. In the next section, the k-Є, Wilcox k-ω, BSL k-ω and SST models will be briefly discussed.

5.1.2 k-Є Turbulence model

The k- Є model solves for two variables: k; the turbulent kinetic energy, and epsilon; the rate of dissipation of kinetic energy. Wall functions are used in this model, so the flow in the buffer region is not simulated. The k-epsilon model is very popular for industrial applications due to its good convergence rate and relatively low memory requirements. It does not very accurately compute flow fields that exhibit adverse pressure gradients, strong curvature to the flow, or jet flow. It does perform well for external flow problems around complex geometries.

The k- Є model introduces k (m^2/s^2) as the turbulence kinetic energy and Є (m^2/s^3) as the turbulence eddy dissipation. The continuity equation remains the same:

$$\frac{\partial \rho}{\delta t} + \nabla \cdot (\rho U) = 0 \tag{5.6}$$

The momentum equation changes, as shown by equation (5.7)

$$\frac{\partial \rho U}{\partial t} + \nabla \cdot (\rho U \otimes U) = -\nabla p' + \nabla \cdot \{\mu_{eff}(\nabla U + (\nabla U)^T)\} + S_M \tag{5.7}$$

Where, S_M is the sum of body forces, μ_{eff} is the effective viscosity accounting for turbulence and p' is the modified pressure. The k-Є model uses the concept of eddy viscosity giving the equation for effective viscosity as shown by equation (5.8):

$$\mu_{eff} = \mu + \mu_t \tag{5.8}$$

μ_t is the turbulence viscosity is linked to the turbulence kinetic energy and dissipation by the equation (5.9):

$$\mu_t = C_\mu \rho \frac{k^2}{\epsilon} \tag{5.9}$$

Where C_μ is a constant.

The values for k and Є come from the differential transport equations for the turbulence kinetic energy and the turbulence dissipation rate.

The turbulence kinetic energy equation is given as equation (5.10):

$$\frac{\partial(\rho k)}{\partial t} + \nabla \cdot (\rho U k) = \nabla \left[\left(\mu + \frac{\mu_t}{\sigma_k} \right) \nabla k \right] + P_k + P_{kb} - \rho \epsilon \tag{5.10}$$

The turbulence dissipation rate is given by equation (5.11):

$$\frac{\partial(\rho \epsilon)}{\partial t} + \nabla \cdot (\rho U \epsilon) = \nabla \left[\left(\mu + \frac{\mu_t}{\sigma_\epsilon} \right) \nabla \epsilon \right] + \frac{\epsilon}{k} (C_{\epsilon 1}(P_k + P_{\epsilon b}) - C_{\epsilon 2} \rho \epsilon) \tag{5.11}$$

Where $C_{\epsilon 1}$, $C_{\epsilon 2}$, σ_k, σ_ϵ are constants.

P_k is the turbulence production due to viscous forces and is modeled by the equation (5.12):

$$P_k = \mu_t \nabla U \cdot (\nabla U + \nabla U^T) - \frac{2}{3} \nabla \cdot U (3\mu_t \nabla \cdot U + \rho k) \tag{5.12}$$

A buoyancy term may be added to the previous equation if the full buoyancy model is used. However, this option is not used in this study.

5.1.3 Wilcox k- ω turbulence model

The k-omega model is similar to k-epsilon, instead however, it solves for omega- the specific rate of dissipation of kinetic energy. It also uses wall functions and therefore has comparable memory requirements. It has more difficulty converging and is quite sensitive to the initial guess at the solution. Hence, the k-epsilon model is often used first to find an initial condition for solving the k-omega model. The k-omega model is useful in many cases where the k-epsilon model is not accurate, such as internal flows, flows that exhibit strong curvature, separated flows, and jets.

This model has an advantage over the k-∈ model, where it does not involve complex linear damping functions for near wall calculations at low Reynolds numbers. The k- ω model assumes that the turbulence viscosity is related to the turbulence kinetic energy, k, and the turbulent frequency, ω, by the equation (5.13):

$$\mu_t = \rho \frac{k}{\omega} \tag{5.13}$$

The transport equation for k is given by the equation (5.14):

$$\frac{\partial(\rho k)}{\partial t} + \nabla \cdot (\rho U k) = \nabla \left[\left(\mu + \frac{\mu_t}{\sigma_k} \right) \nabla k \right] + P_k + P_{kb} - \beta' \rho k \omega \tag{5.14}$$

The transport equation for ω is shown as equation (5.15):

$$\frac{\partial(\rho \omega)}{\delta t} + \nabla \cdot (\rho U \omega) = \nabla \cdot \left[\left(\mu + \frac{\mu_t}{\mu_\omega} \right) \nabla \omega \right] + \alpha \frac{\omega}{k} P_k + P_{wb} - \beta \rho \omega^2 \tag{5.15}$$

The production rate of turbulence (P_k) is calculated as shown previously in the k-∈ section.

5.1.4 Shear stress transport model

SST model is a combination of the k-epsilon in the free stream and the k-omega models near the walls. It does not use wall functions and tends to be most accurate when solving the flow near the wall. The SST model does not always converge to the solution quickly, so the k-omega models often solved first to give good initial conditions.

The k- ω based Shear Stress Transport (SST) model of Menter was applied for turbulence treatment. The transport equation for the SST model are expressed below where the turbulent kinetic energy 'k' and turbulent frequency or dissipation per unit turbulent kinetic energy 'ω' are computed by using the following relations:

For Turbulence Kinetic Energy,

$$\frac{\partial k}{\partial t} + \nabla \cdot (uk) = P_k - \beta^* k \omega + \nabla \cdot [v + \sigma_k v_T] \nabla k \tag{5.16}$$

Where, P_k is the production limiter.

For Specific Dissipation Rate,

$$\frac{\partial \omega}{\partial t} + \nabla \cdot (u\omega) = \alpha S^2 - \beta \omega^2 + \nabla \cdot [(v + \sigma_\omega v_T) \nabla \omega] + 2(1 - F_1) \sigma_{\omega 2} \frac{1}{\omega} \nabla k \nabla \omega \tag{5.17}$$

The first blending function F_1 is calculated from

$$F_1 = \tanh\left\{\left\{min\left[max\left(\frac{\sqrt{k}}{\beta^*\omega y};\frac{500v}{y^2\omega}\right)\frac{4\rho\sigma_{\omega 2}k}{CD_{k\omega}y^2}\right]\right\}^4\right\} \quad (5.18)$$

$$CD_{k\omega} = max\left(2\rho\sigma_{\omega 2}\frac{1}{\omega}\nabla k.\nabla\omega.10^{-10}\right) \quad (5.19)$$

And, Kinematic eddy viscosity,

$$\nu_T = \frac{\alpha_1 k}{\max(\alpha_1\omega, SF_{2)}} \quad (5.20)$$

Where, S is the invariant measure of the strain rate and F_2 is the second blending function expressed as:

$$F_2 = \tanh\left[\left\{max\left(2\frac{\sqrt{k}}{\beta^*\omega y};\frac{500v}{y^2\omega}\right)\right\}^2\right] \quad (5.21)$$

Each of the constants is a blend of an error of an inner (1) and outer (2) constant, blended through

$$\emptyset = \emptyset F_1\emptyset_1 + (1 - F_1)\emptyset_2 \quad (5.22)$$

Where, $\emptyset_1$ and $\emptyset_2$ are the coefficients of the k-ω and k-∈ models respectively.

The turbulence viscosity is calculated by,

$$v_T = min\left(\frac{\rho k}{\omega}, \frac{a_1\rho k}{SF_2}\right) \quad (5.23)$$

Where $a_1 = 0.31$ and blending function F_2 is obtained from equation (4.21).

5.2 Modeling

3D modelling of the components were generated in Solidworks 2016 according to the available designs. The runner contained 15 blades with the inlet angle of 15 degrees having fixed guide vane. Figure 5.1 shows the 3D overall set up and model of Francis turbine.

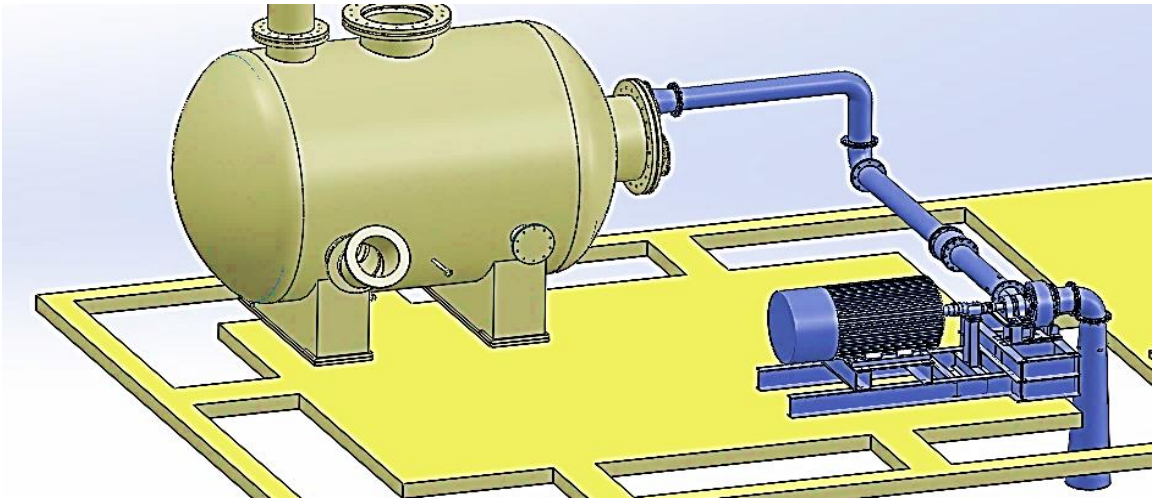

Figure 5.1 3D Drawing of Setup

5.2.1 Mesh Generation

Mesh generation is done to create a numerical domain over a geometric feature in which the computer solves the required equations. ICEM CFD allows for the generation of several structured and unstructured meshes. Generally used meshes are tetrahedral and hexahedral. Tetrahedral meshes are easy to resolve and it computer takes less time solve the equations whereas hexahedral meshes are time consuming and the result provided by hexahedral meshes are of high quality.

For the calculation, the computational domain has been divided into several sections as spiral casing, vanes, runner, and draft tube. Hexahedral meshing has been done in the runner to ensure the quality of the results. Tetrahedral meshes on the other components satisfy the required quality of the result and reduce computational time. The primary results and performance curve has been generated by the mesh created as above. The whole computational grid comprises of ---- million meshes. Mesh refinement and boundary layer was inserted to obtain the required quality of mesh and to allow smooth transitions of mesh between the domains.

However, for the optimization propose single blade passage has been considered after verification of the results with full domain. The single blade passage reduces computational time and allows effective optimization simplicities in the blade. Turbo Grid has been used to generate meshes of required quality for optimization propose. Total number of grids is comprised of 0.15 million meshes for a single blade passage. Fig 5.1 shows the mesh discretization, boundary layer, grid interfaces created in the domain etc.

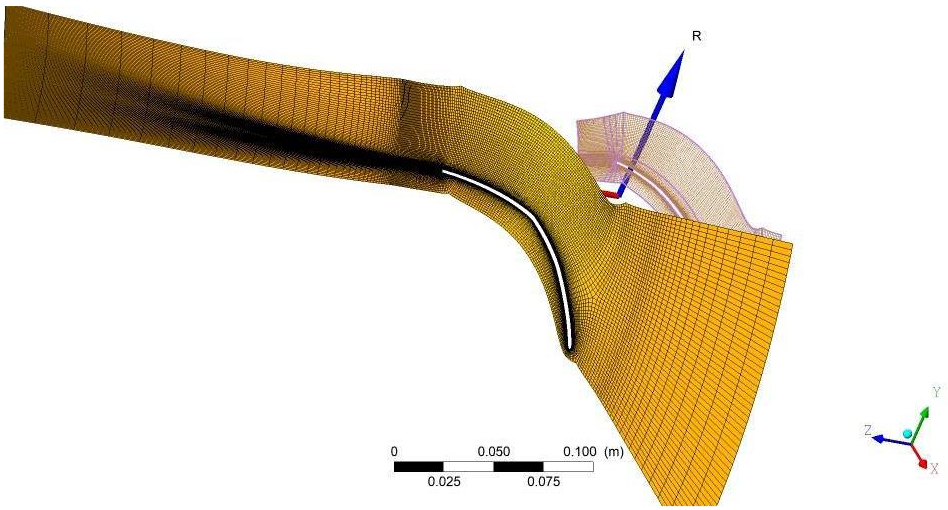

Figure 5.2 Mesh generation in Single Blade Passage

5.2.3 Mesh Independence Study

The solution of a domain depends on the number and quality of meshes in the geometry. Large number of mesh increases the computational time and predicts the solution accurately as the solution is resolved in smaller cells. However, it is necessary to find the minimum number of meshes required for the geometry for the solution to be independent on the number and types of meshes. This minimum number of mesh has then been used for the computation so that it predicts the solution accurately and requires the minimum possible computational time for the solution to converge. The number of mesh in full turbine reference domain has been changed from 1 million to 5 million by increasing at a rate of 1.3. The number of mesh for design optimization, single blade passage has been increased from 0.08 million to 0.1 million increasing at a rate of 1.3.

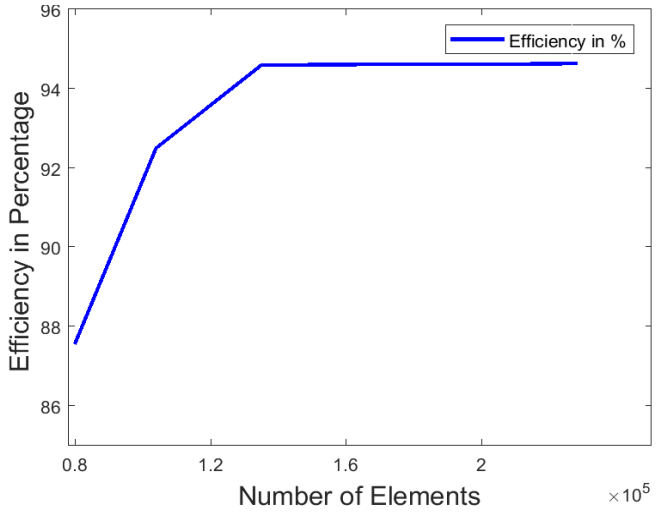

Figure 5.3 Mesh Independence for Single Blade Passage

Fig 5.2 shows the mesh independence study of reference turbine. Fig 6.2 shows the mesh independence study in single blade passage. Table 6.1 includes the summary details of meshes used for the computation in both the domains.

Table 5.1 Summary of Mesh Statistics

Details	Full Turbine	Single Blade Passage
Type of Mesh	Hexahedral in runner , Tetrahedral in other components	Hexahedral in Blade
Number of Elements	3278971	451421
Number of Nodes	4178115	254788

5.3 Numerical Approach

The commercial 3D Navier-Stokes CFD solver ANSYS (2018) CFX was used to analyze the performance of the turbine. Steady State incompressible flow having a single fluid water in the direction along the inlet of the spiral casing was used for whole domain whereas the cylindrical component of inlet was given for the single blade passage. The radial and theta components at the inlet of the blade passage were given. At the inlet and outlet, pressure inlet as well as pressure outlet was given converting the required head into pressure. Total pressure at the inlet and static pressure outlet was given. Shear Stress Transport (SST) model, which accounts for the transport of turbulent shear stress and gives highly accurate predictions of the onset and the amount of flow separation under adverse pressure gradients, is used.[12]

Regarding the numerical treatment between the stationary and the rotating components frozen rotor is used for the runner. Two interfaces are inserted. One between the vanes outlet and the runner inlet and other between the runner outlet and the draft tube inlet. This model produces a steady state solution to the multiple frame of reference problems, with some account of the interaction between the two frames [12].

With the physical time step of 0.1 sec, convergence criteria of RMS $1*10^{-3}$ residual were considered for maximum of 100 iterations to achieve the solution of acceptable level. Cavitation and erosion model was not considered in this simulation. Performance analysis was done for the reference turbine by varying the discharge and rpm and inference were made. All simulations were performed using ANSYS CFX in parallel network workstation. The setup for the overall domain is shown in the Figure 5.4 and domain for optimization is shown in Figure 5.5 also the boundary conditions are summarized in Table (5.2) below.

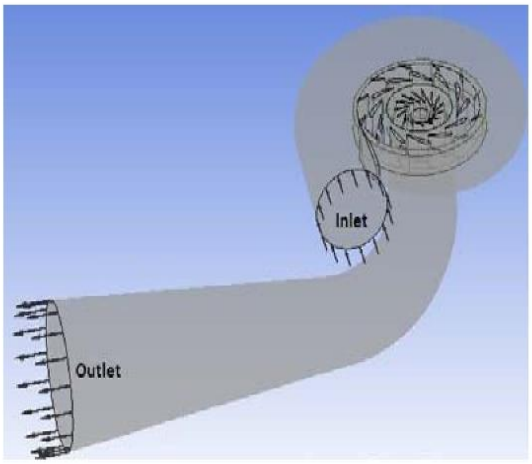

Figure 5.4 Full turbine setup

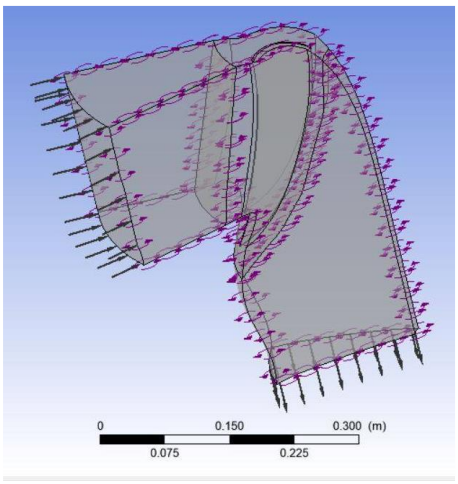

Figure 5.5 Single Passage Setup

Table 5.2 Summary of Computational Domain Setup

Summary	**Full Turbine setup**	**Single Blade Passage**
Inlet	Total Pressure (2.6 atm)	Total Pressure (2.6 atm)
Outlet	Static Pressure (1 atm)	Static Pressure (1 atm)
Turbulence Model	SST	SST
Maximum iteration	100	100
Type	Single phase steady state	Single phase steady state

CHAPTER 6 Results and Discussions

6.1 Performance curves by the variation of rotor speed

Numerical analysis was done for the reference turbine by varying the speed of the turbine having all other conditions unchanged. Fig 6.1 shows the plot of efficiency of the turbine at varying speed. Performance curves show that the turbine has maximum efficiency of 94% at 1450 rpm respectively. The nature of the performance curves suggest that the efficiency increases from 1100 rpm to 1450 rpm and there is a decrease in efficiency later. This also suggest the suitability of low head Francis turbine at a speed range of 1000 to 1500 rpm.

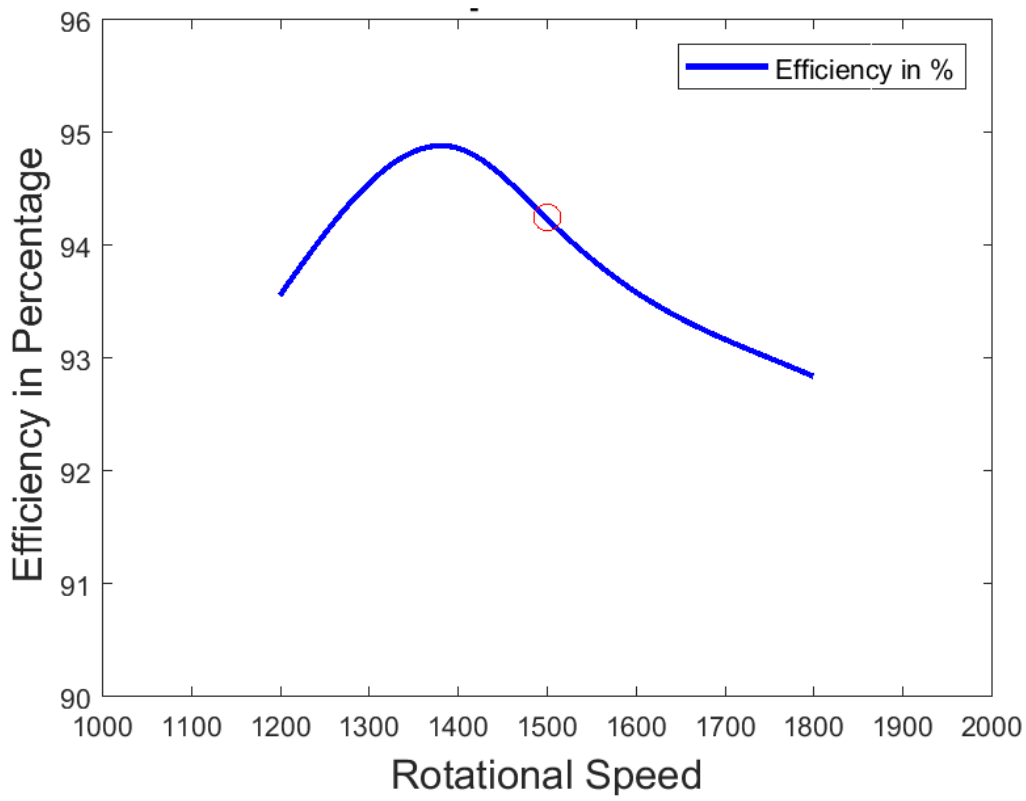

Figure 6.1 Performance characteristics of Reference Turbine at varying speed

6.2 Performance curves by the variation of flow rate

Numerical analysis was done for the reference turbine by varying the flow rate from 0.09 m^3/s to 0.1 m^3/s of the flow conditions. Fig 6.2 shows the plot of efficiency of the turbine at varying flow rates. Performance curves depict that the efficiency increases from 0.09 m^3/s to 0.098 m^3/s and then the efficiency decreases. The curve has a steep slopes in both the part load as well as full load conditions.

An important illustration can been seen as for the fixed guide vane turbines the flow variation range is shorter the efficiency curve is steeper at full load conditions than at part load.

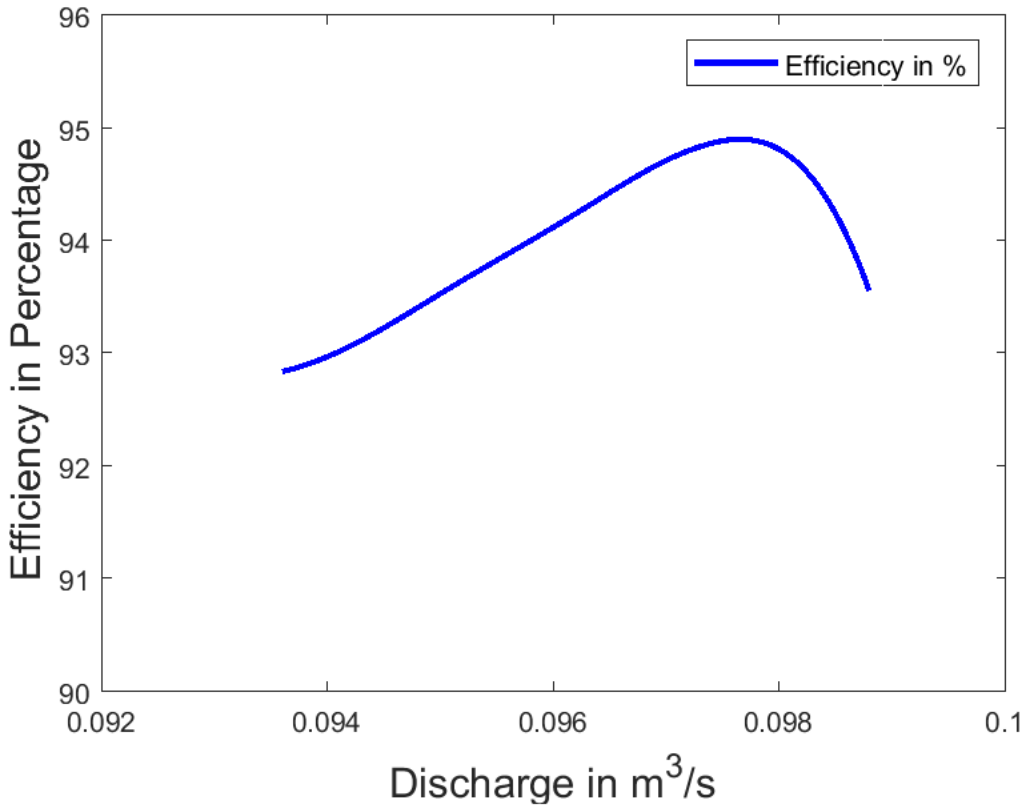

Figure 6.2 Performance Characteristics of Reference Turbine at Varying Discharges

6.3 Effect of the turbulence models

Turbulence modeling is a key issue in most CFX simulations. Turbulence models are used to predict the turbulent flow effects of a fluid flow without resolving the small scale fluctuations. These models are based on RANS (Reynolds Averaged Navier- Stokes) equations. In some domain turbulent models has large impacts due to the some limitations in every models. So it is very important to use the turbulent modeling that gives most accurate results with less error depending upon the fluid domain. Most commonly used turbulent models in ANSYS CFX are k-∈, k- ω, and SST models. K-∈ model is used for general applications due to its accuracy and robustness. However, it does not provide good prediction of the boundary layer separation and flow separation in rotating fluids. The k- ω based Shear Stress Transport (SST) model provides an accurate prediction of the flow separation under adverse pressure gradients. Since this model is developed to overcome deficiencies of both k-∈ and k- ω model, SST model is more advanced (25). Six different types of turbulence model viz; k-epsilon, k-omega, RNG k-epsilon, SST, BSL, Laminar (no turbulence) were tried.

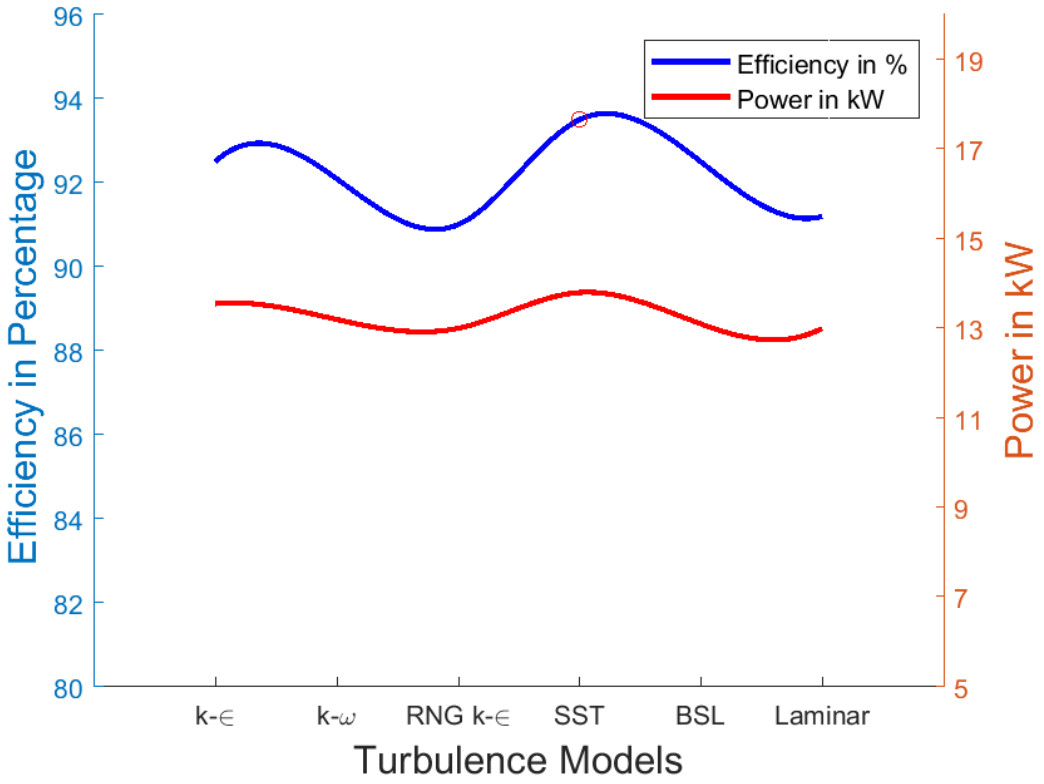

Figure 6.3 Effect of Various Turbulence Models

Fig 6.3 shows the shaft power output and efficiency of the reference turbine obtained for different turbulence models used for simulations. The results from the simulations show that the efficiency varies from a range of 91% to 94 % in these models. The variation in the efficiencies due to the turbulence models are because of the specific limitations of each turbulence models. Different equations are solved in different models to obtain a solution so a model with higher accuracy and adaptability with the flow domain needs to be adopted. The highest efficiency is obtained as 94% with a shaft power output of 13.5 kW using SST turbulence models. The SST model predicted the flow behavior more accurately so for all the simulations, SST turbulence model has been adopted.

6.4 Performance curve Experimental and Computational calculations

Efficiencies at varying speed of the rotor and varying flow rate for both the computational as well as experimental results for the reference turbine has been discussed in this section. As the experiment is done for two runners i.e, casted and forged runner so the performance of both has been discussed.

Fig 6.4 shows the experimental and numerical study of the reference turbine at varying rotor speed from 600 to 1800 rpm. The nature of the curves show similar pattern for both the

numerical and experimental cases, with a maximum efficiency of around 1300 to 1500 rpm. However the differences in the efficiencies and shaft power output in the computational and experimental may have arouse due to the manufacturing defects, mechanical losses, measurement uncertainties, etc.

However, the graph shows a better performance is obtained for the forged runner than the casted runner for same operating conditions due to the manufacturing accuracy obtained in the forging process. Maximum efficiency is obtained as 94 % in computation at 1400 rpm and whereas maximum efficiency is obtained as 76 % in experiment at 1450 rpm. This shows a closer agreement between computation and experiment.

The nature of curves in both numerical and experimental analysis is similar and the trend is obtained with an increasing efficiency up to around 1500 rpm and a steep change in efficiency at other rpms. Decrease in efficiency at higher rpm during the experiment may be accounted due to the vibration in the set-up and heating problem in the motor. The relative error for efficiencies between the computational and experimental cases for forged and casted runner at design rpm has been obtained as 22% and 26% respectively.

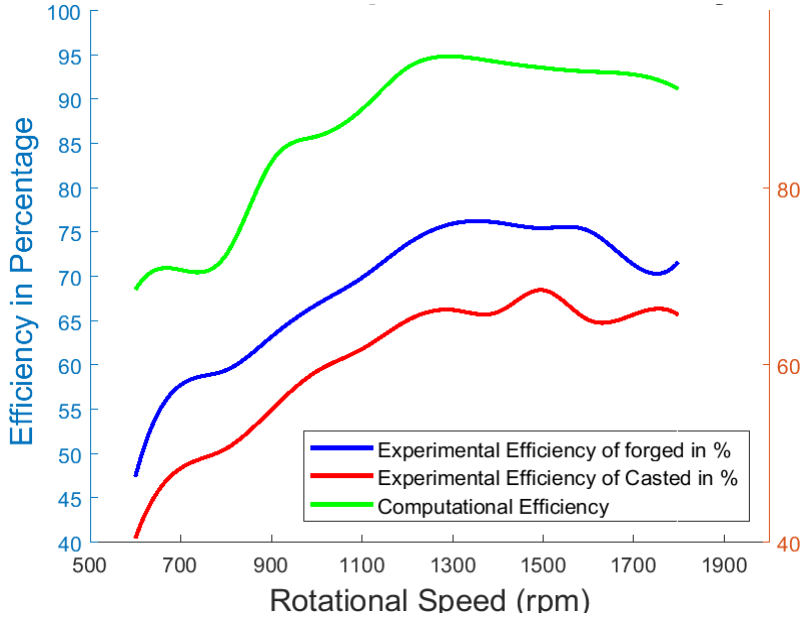

Figure 6.4 Comparison of Efficiency for Computation and Experimentation at Varying Speed

Fig 6.5 shows the experimental and numerical study of the reference turbine at varying flow rate conditions. The nature of the curves show similar trends for both the numerical and experimental studies with a peak efficiency of 93 % in computation at 0.094 m^3/s discharge and -77% in experiment at 0.093 m^3/s discharge respectively. The trend shows that the nature of the curve increases gradually till the maximum efficiency point and decreases steeply later.

The limitation for this experiment and computation was the maximum and minimum discharge feasible in the set-up and certain rpm of the rotor. The efficiency plot for a fixed guide vane has been found to be for a shorter range as above and below certain discharges the trends are erratic in both computation and experimentation. From this result we can say that the range of flow variation for a Francis turbine at fixed guide vane opening is minimal.

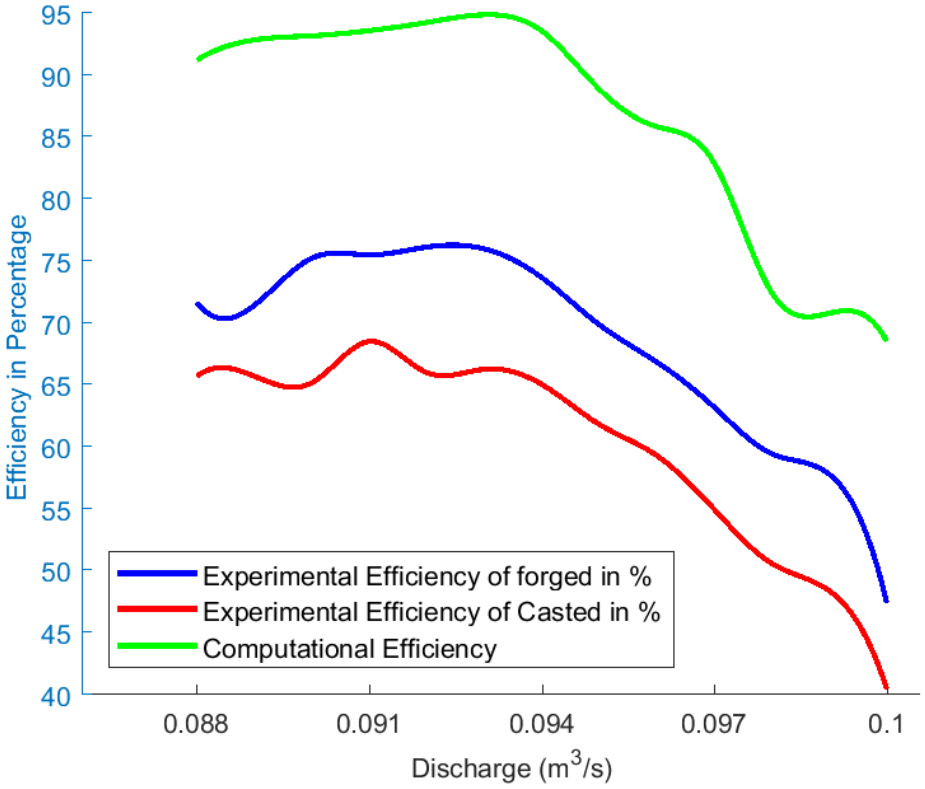

Figure 6.5 Comparison of Efficiency for Computation and Experimentation at Varying Discharges

There is a difference in the experimental and computational analysis. This may be due to the mechanical losses, experimental uncertainties, etc. in the set-up.

Fig 6.6 shows the change in discharge at varying rpm. An interesting observation in the computation was observed for Francis turbine as the nature of the curves is quite different at certain limits. At increasing rpm the discharge for Francis turbine is expected to decrease which is obtained in both the computation and experiment. However, for decreasing rpm from BEP the discharge is expected to increase which is obtained for both computation and experiment up to a certain decrement in rpm. But, this increase in discharge is not obtained and the discharge starts to decrease after a critical rpm which is obtained as 1200 rpm in computation and around 1100 rpm during experiment.

The change in discharges due to the change in rpm is governed by the change in centrifugal force due to the change in rpm of the rotor. The micro Francis runner shows a mixed turbine nature i.e, radial and axial for certain range and shows axial nature after a critical value.

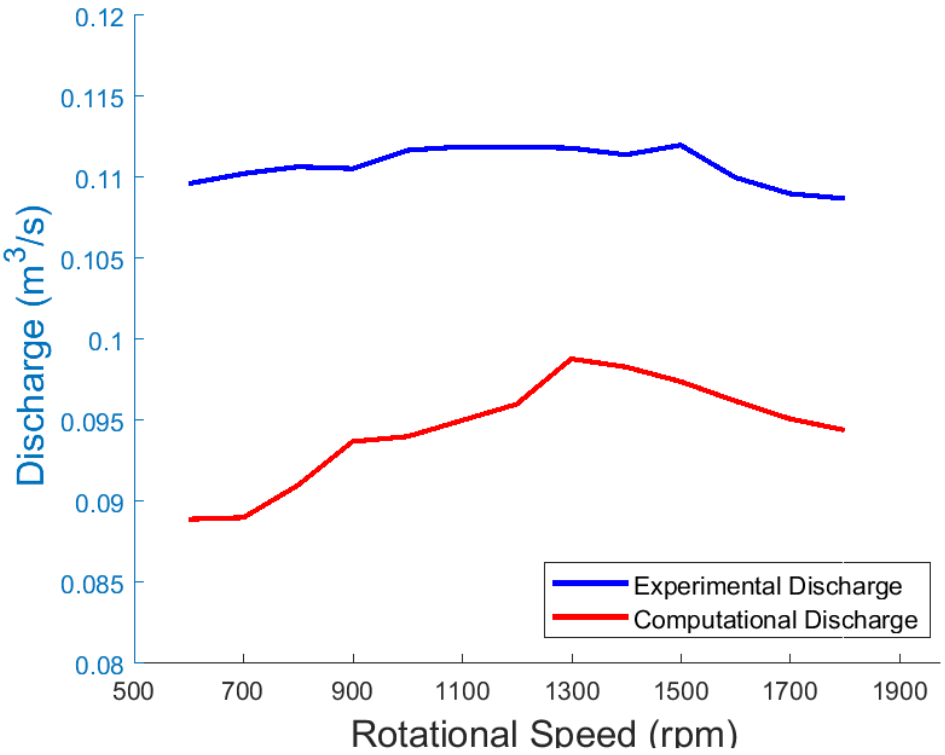

Figure 6.6 Comparison of Computation and Experimental Discharges at Varying Speed

The difference in discharges at same speed for computation and experiment may have been resulted due to the frictional forces, surface roughness and other mechanical forces which have not been considered for computation.

CHAPTER 7 DESIGN OPTIMIZATION OF THE FRANCIS RUNNER BLADES

The performance of a turbine is characterized by its efficiency, which is a measure of the output energy produced to the input energy. Single turbine has different efficiencies at varying input energy. The variation of maximum efficiencies over wide range of operating conditions show that the parametric effects of geometric and physical factors on efficiency. By physical it means the vibration, heating problem, frictional losses and mechanical losses in the turbine. By geometrical factors it means the effect of blade shape, blade inlet and outlet angle, ratio of inlet and outlet diameters, blade lean, and energy conversion throughout the blade which is governed by beta distribution, blade thickness and blade number [13].

During the process of design optimization, blade lean and beta distribution has been changed and its effects on blade shape and performance has been investigated through numerical study. For every optimization process only one parameter has been changed keeping all other constant as reference to identify the parametric effect.

7.1 Blade Lean Change

Lean is the degree of hub or shroud line shifted from the original position (Gjosaeter 2011). Lean is an important parameter for controlling the pressure balance in the runner. During optimization, blade lean has been changed with different lean angles of -10 to +30 degrees having an interval of 5 degrees. All the models were simulated and the results were compared with the reference model. Table 7.1 lists all the cases of lean angle changes. Fig 7.1 shows the changes in the blade shape from the reference shape due to the introduction of lean angle.

Table 7.1 Various Cases of Blade Lean

Case No.	**Lean Angle (degrees)**
1	-10
2	-5
3	-0
4	5
5	10
6	15
7	20
8	25
9	30

7.1.1 Positive blade lean change

The positive linear lean defined on the blade causes a twisting in the blade from the shroud in the direction of rotation. The location of water heating the leading edge of the blade changes because of the lean angle. Introducing a positive lean in the blade causes water to strike on the pressure side of the blade. This changes the vector plots of the streamlines along the blade. When there is a lean in the direction of rotation, the pressure distributions on the suction side and the pressure side is more uniform.

7.1.2 Negative blade lean changes

The negative linear lean defined on the blades cause twisting of blade from the shroud against the direction of rotation. Introducing a negative lean in the blade causes water to strike on the suction side of the blade. The original design has a leading edge cavitation at the suction side of the blade, this negative pressure zone expands and makes the blade prone to cavitation damage when there is a lean in the reverse direction.

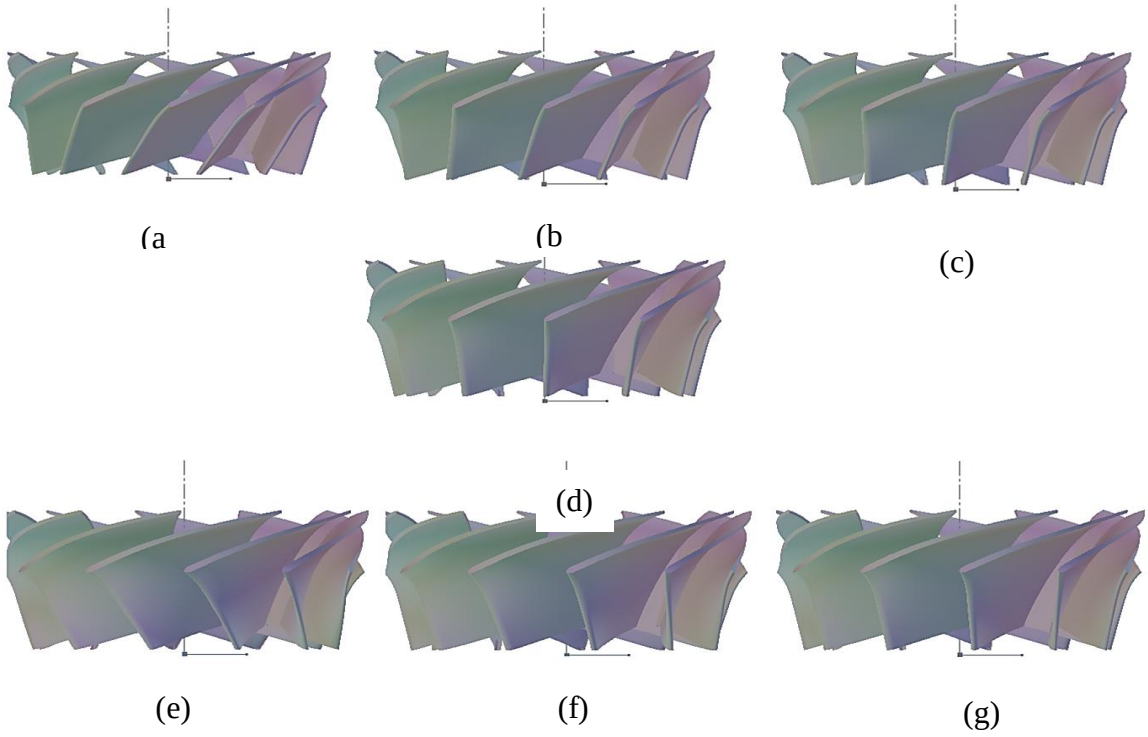

Figure 7.1 Shape modification due to Lean angle (a) -20^0 lean (b) -10^0 lean (c) -5^0 lean (d) 0^0 lean (e) 20^0 lean (f) 10^0 lean (g) 5^0 lean

7.1.3 Performance curves

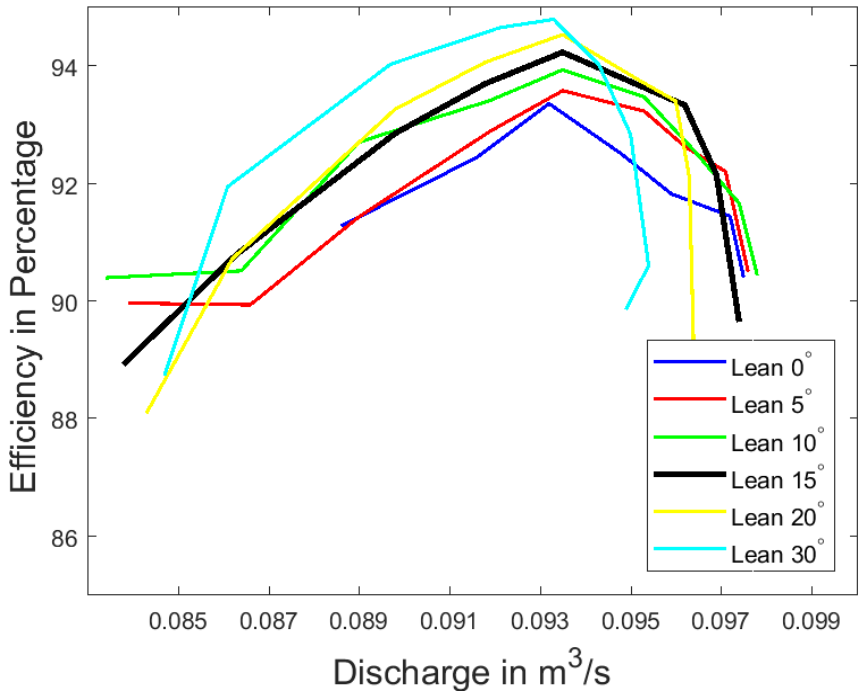

Figure 7.2 Effect of Lean on Performance of Turbine

Fig 7.2 shows the efficiency of the reference blade and modified turbine with various blade leans. The nature of the efficiency curves depicts that it increases efficiency from the reference

model as positive lean angle is introduced. But, with further increase in blade lean the operating range of the turbine is decreased than the reference turbine. An efficiency of 94% was obtained with lean at 15 degrees with an increase of peak efficiency of 2% from the reference turbine.

7.2 Beta Distribution

The shape of the runner blade is dependent on the beta angle distribution from the leading and trailing edge. The beta distribution for the low head Francis turbine is not determined exactly. Beta distribution has a direct effect on the energy conversion in the blade. The distribution also governs significantly the blade loading on the blade. Reference turbine has a linear blade distribution which gives uniform energy conversion along the blade. Two other distribution of blade beta angle has been seen and numerical results have been analyzed keeping the inlet and outlet angle constant.

7.2.1 Sinusoidal Beta Distribution

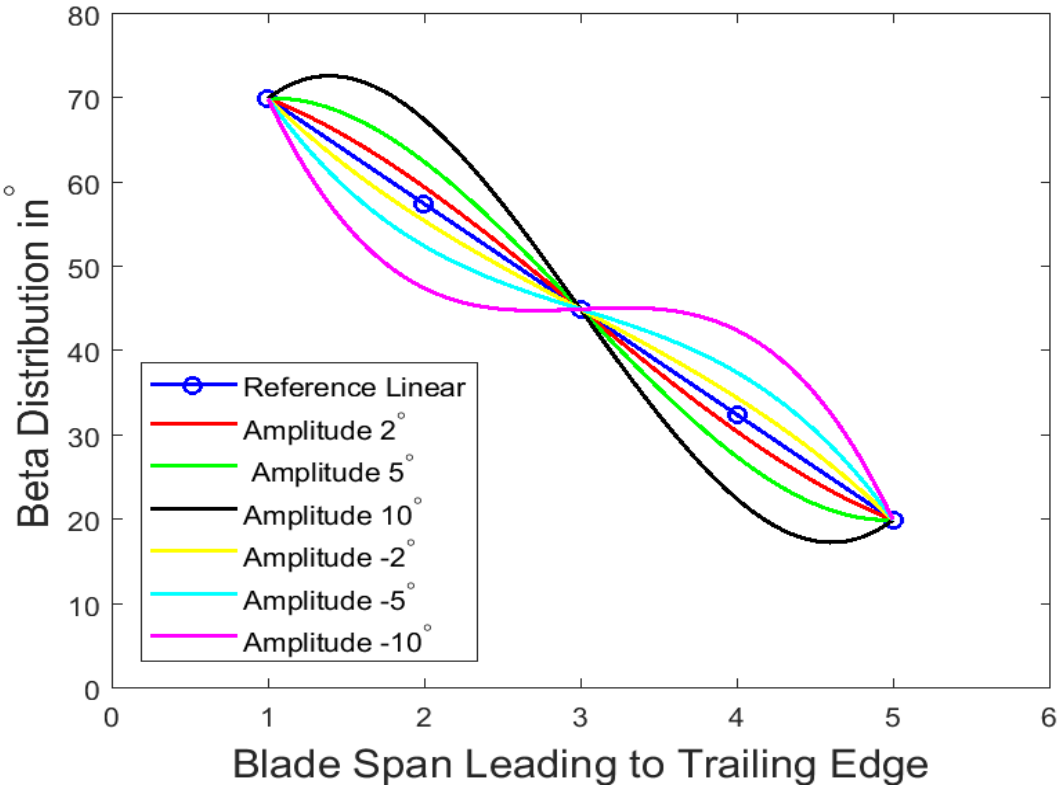

Figure 7.3 Sinusoidal Beta Distributions

Fig 7.3 shows the sinusoidal and reference beta distribution in the runner. The sinusoidal beta distribution also has positive and negative amplitudes from the midpoint of the blade. The positive distribution has an increasing beta angle starting from the leading edge and decreasing at the trailing edge. This beta distribution has more energy conversion in the first half of the

blade and lesser energy conversion at the back half. Increasing the amplitude of sinusoidal beta distribution causes a rapid shift in the beta change at the middle section of the blade.

The negative distribution has a decreasing beta angle starting from leading edge and increasing at the trailing edge

Figure 7.4 Blade to Blade View of Runner having Sinusoidal Beta Distribution

(a) (b)

Fig 7.4 shows the blade to blade span view of blades for reference turbine and modified turbine having sinusoidal beta distribution with positive (a) and negative (b) amplitudes.

7.2.2 Performance curves

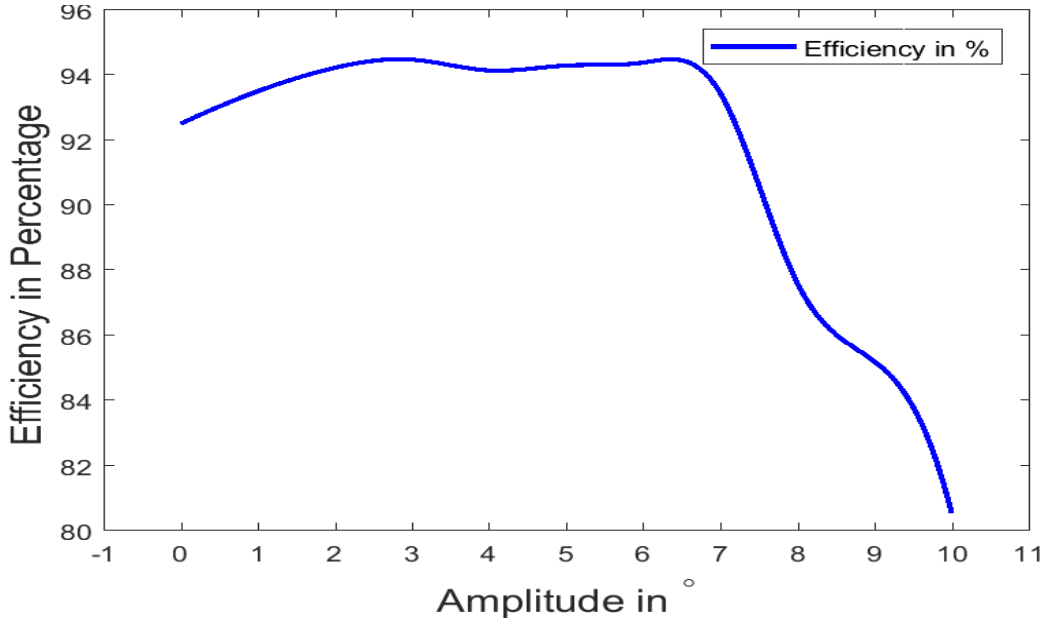

Figure 7.5 Performance Curve of modified runner having sinusoidal beta distribution

The curves depicts that having a positive distribution increases the efficiency and has better performance up to a certain limit and there is sudden drop in efficiency on higher amplitudes. This is due to the sudden shift of beta angle at the midpoint of the blade resulting in the occurrence of inter blade vortices from the hub to the shroud as seen in Fig 7.6.

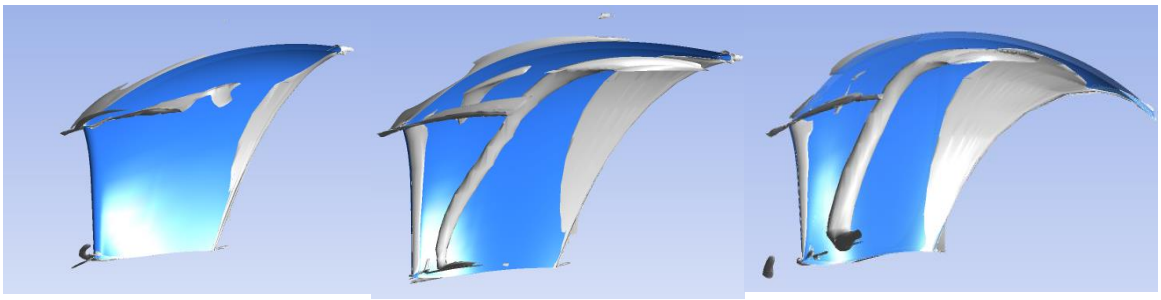

Figure 7.6 Inter blade Vortex rope seen at higher amplitudes of sinusoidal beta distribution

Sinusoidal beta distribution shifts the operating range of the turbine as the shape of the blades is modified. The performance curve shows that sinusoidal beta distribution having an amplitude less than the critical limit can enhance the performance.

7.2.3 Parabolic Beta Distribution

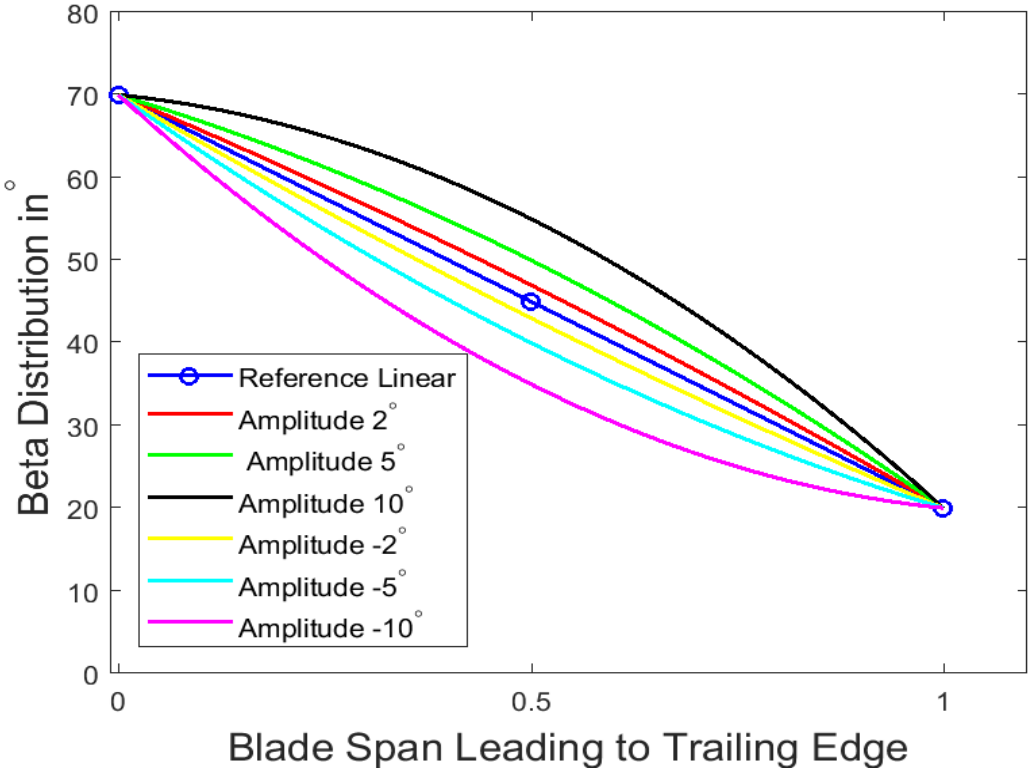

Figure 7.7 Parabolic Beta Distribution

Fig 7.7 shows the parabolic and linear beta distribution of the modified and reference runner respectively. The parabolic distribution also has positive and negative amplitudes. The amplitude is varied from the midpoint keeping the inlet and outlet angle constant. Parabolic distribution has a significant change in the blade length.

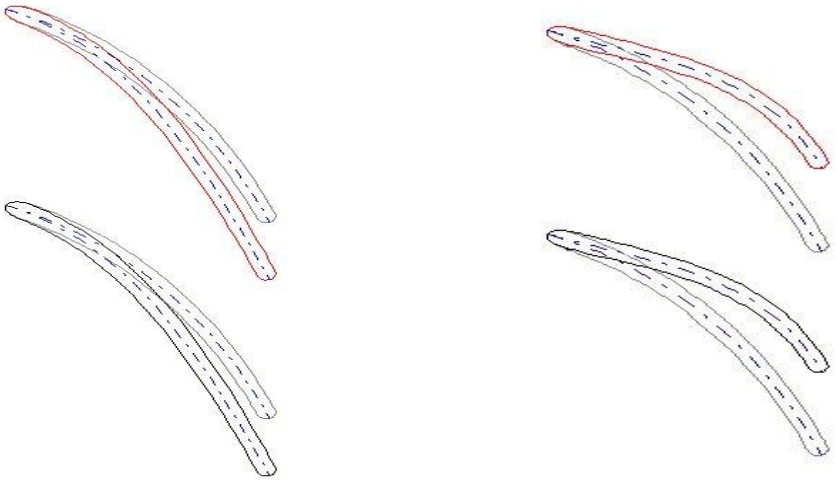

Figure 7.8 Blade to Blade view of Runner having parabolic beta distribution

Fig 7.8 shows the blade to blade span view of runner blades having parabolic beta distribution with positive (a) and negative (b) amplitudes.

7.2.4 Performance curves

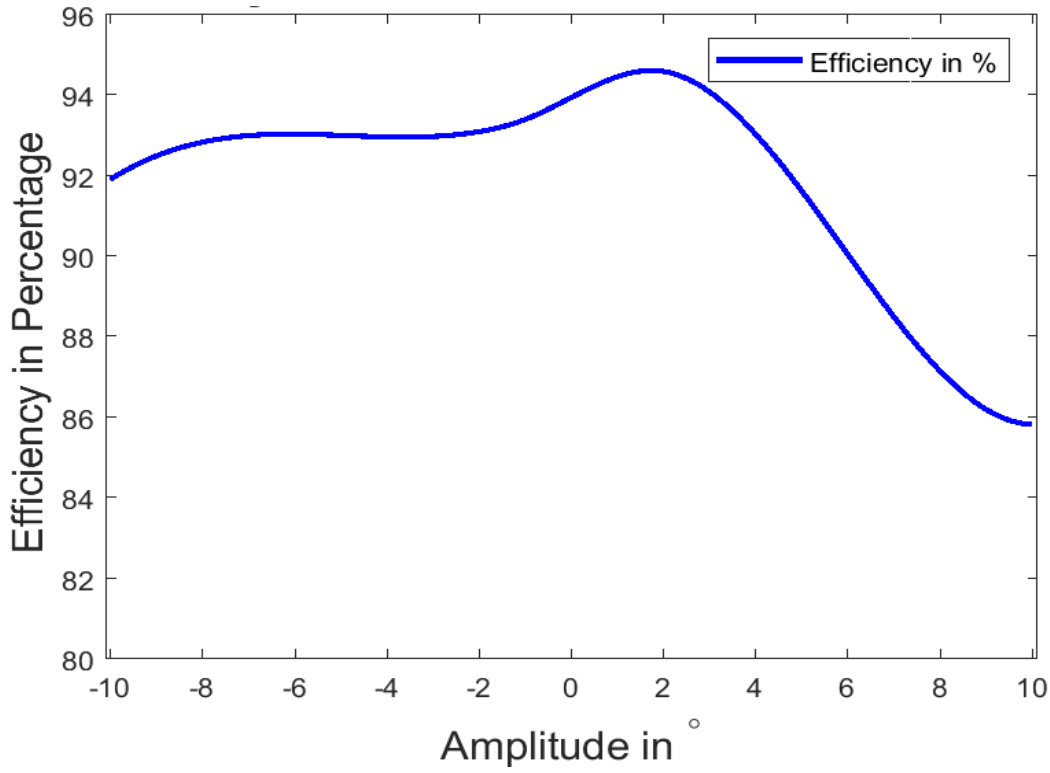

Figure 7.9 Performance Curve of runner having parabolic distribution of varying amplitudes

Fig 7.9 shows the performance curves of Francis runner having parabolic beta distribution. The distribution is varied from -10 to 10 degrees. With the introduction of positive parabolic distribution the blade shape at the trailing edge is increased. There is a limit in the negative amplitude of parabolic distribution as decreasing the amplitude causes the blades at trailing edge to intersect. The operating range shifts towards the part load conditions with a better performance due to larger length and complete energy conversion.

7.3 Optimized Runner

Both blade lean and beta distribution has effects in the performance of the runner. The effect of both these parameters have been combined to obtain an optimized runner. Fig (7.10) shows the shape of the optimized runner which has a lean 15 degrees and parabolic distribution having an amplitude of 2 degrees.

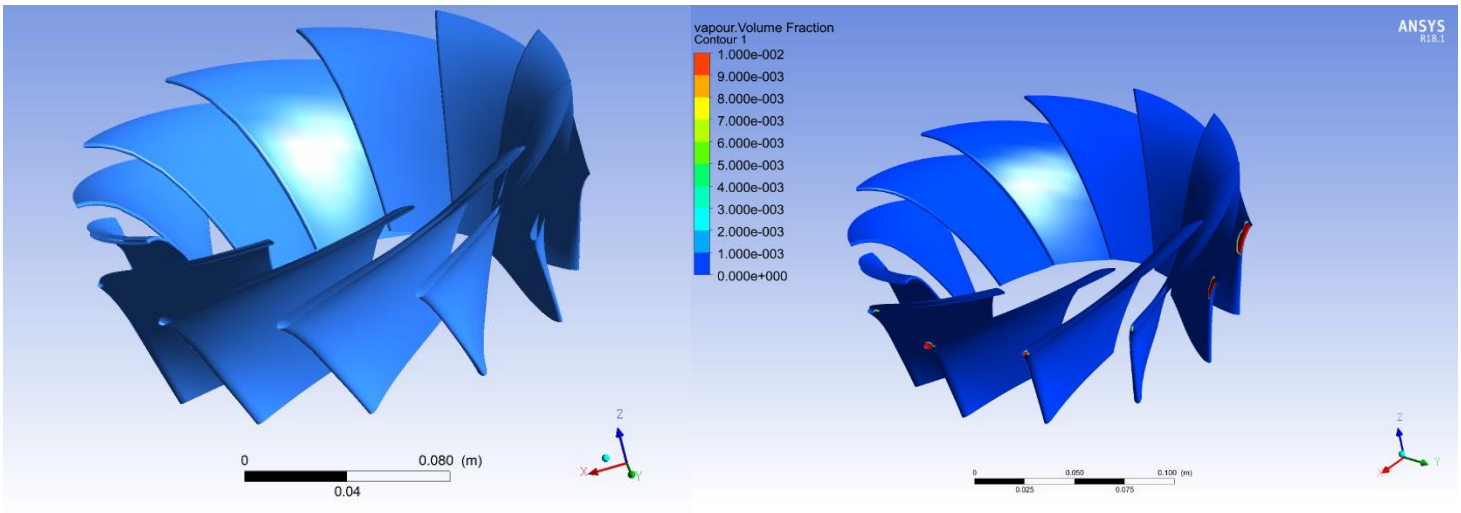

Figure 7.10 Shape comparison of Runners

Fig 7.10 shows the shape of reference runner(b) and optimized runner(a) along with leading edge cavitation seen in the reference runner and optimized runner without leading edge cavitation.

Fig 7.11 shows the comparison of performance curve of reference runner and the optimized runner.

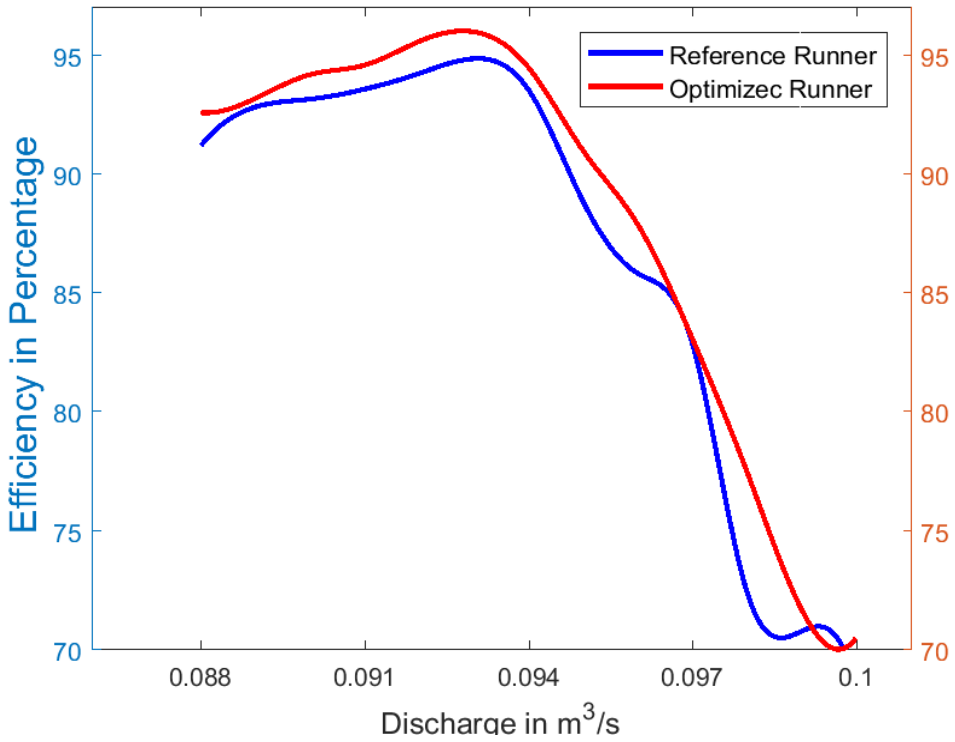

Figure 7.11 Comparison of Performance Curve of Reference and Optimized Runner

The performance curves depicts an increase in efficiency of about 2% at the BEP and increase of around 1% efficiency at both the full load and part load conditions. Thus the optimized runner has a better performance over all operating range of the runner. The optimized runner also has no leading edge cavitation which was seen in the reference runner.

CHAPTER 9 CONCLUSION

This research work focuses on the performance analysis of the Francis turbine both numerically and experimentally with its design optimization numerically. At the design speed 1500 rpm for specified guide vane opening angle, experimental data show the efficiency of 76 % whereas the numerical results show 94%. The best efficiency was obtained at 1450 rpm from both experiment and simulation which shows agreement of the design process.

The forged runner has a better efficiency of 8% than the casted runner due to the manufacturing procedures and dimensional accuracies. The surface roughness and thickness of the blade in the casted runner may have caused its performance to be lower.

The lean angle can solve the leading edge cavitation as it changes the point at which water strikes the blade. The pressure fluctuation at the inlet also can be limited by the introduction of lean angle. Lean angle shows significant effects on low head Francis turbine

Beta distribution has primary effects on blade loading and a frontal loading shall be preferred. Parabolic and sinusoidal distributions show better performance over the operating range. However the amplitudes of distribution shall be limited to less than 10 degrees. The blade angle at any point in the blade should be kept lower than the outlet blade angle to prevent sudden pressure fluctuation in the runner which sets the limit for decreasing the amplitude of distribution.

The fixed vane opening of Francis turbine limits the operating range of the turbine to 90% - 110% beyond which the turbine behaves abruptly. However the simplicity and operational efficiency seems to make it useful for power plants with almost a constant flow.

The results and conclusions drawn from the experiment may be affected by the computational and experimental uncertainties which has been limited. The parametric effects and performance analysis of a Francis runner along with the optimized design has been addressed in this thesis.

REFERENCES

[1] K. Gjøsæter, "Hydraulic Design of Francis Turbine Exposed to Sediment Erosion," no. August 2015, 2012.

[2] C. Vi, L. Frøyd, K. Gjøsæter, and O. G. Dahlhaug, "Development of Design Tool for Low-Head Francis Turbine," 2016.

[3] Y. Enomoto, S. Kurosawa, and H. Kawajiri, "Design optimization of a high specific speed Francis turbine runner," *IOP Conf. Ser. Earth Environ. Sci.*, vol. 15, no. PART 3, 2012.

[4] U. Shrestha, Z. Chen, and Y. Choi, "Study on the effect of the runner design parameters on 50 MW Francis hydro turbine model performance Study on the effect of the runner design parameters on 50 MW Francis hydro turbine model performance," 2018.

[5] M. Kaniecki and Z. Krzemianowski, "CFD analysis of high speed Francis hydraulic turbines," vol. 131, no. 131, pp. 111–120, 2016.

[6] F. Ayancik, K. Celebioglu, and S. Aradag, "Parametrical and Theoretical Design of a Francis Turbine Runner," *10th Int. Conf. Heat Transf. Fluid Mech. Thermodyn.*, no. July, pp. 775–780, 2014.

[7] A. Skotak, J. Mikulasek, and J. Obrovsky, "Development of The New High Specific Speed Fixed Blade Turbine Runner," vol. 2, no. 4, pp. 392–399, 2009.

[8] Z. Ma, B. Zhu, C. Rao, and Y. Shangguan, "Comprehensive Hydraulic Improvement and," 2019.

[9] E. Kocak, S. Karaaslan, N. Yucel, and F. Arundas, "A Numerical Case Study: Bovet Approach to Design a Francis Turbine Runner," *Energy Procedia*, vol. 111, no. September 2016, pp. 885–894, 2017.

[10] F. Duparchy, J. Brammer, K. P. Shrestha, and S. Chitrakar, "Study on the effect of the runner design parameters on 50 MW Francis hydro turbine model performance Study on the effect of the runner design parameters on 50 MW Francis hydro turbine model performance," 2018.

[11] N. Water Power Laboratory, "High Head Hydraulic Machinery," 2009.

[12] E. Krämer, "Computational fluid dynamics," *High Perform. Comput. Sci. Eng. '15*

Trans. High Perform. Comput. Center, Stuttgart 2015, pp. 293–300, 2016.

[13] C. N. Mun, D. C. Ba, X. J. Yue, and M. Il Kim, "Multi-objective Optimization of Draft Tube in Francis Turbine Using DOE, RBF and NSGA-II," *Doi.Org*, no. April, pp. 1–13, 2017.

APPENDIX I

Paper Conference Proceedings

The 2nd IAHR-Asia Symposium on Hydraulic Machinery and Systems

24th - 25th September 2019, Busan, Korea

IAHR-Asia 2019-***

A Simplified Francis Turbine for Micro Hydro Applicatin: Design and Numerical Analysis

D.R. Dahal[1], N. Paudel[1], S. Chitrakar[1], B.S. Thapa[1], H.P. Neopane[1] and B. Thapa[1]*

[1] Department of Mechanical Engineering,

Dhulikhel, 44600, Nepal

* Corresponding author. Tel.: +977 980 127 0065, bhola@ku.edu.np

Abstract

Francis turbine is the most widely used type of hydro turbine due to its high efficiency and a wide range of operation. Despite its popularity in large scale power plants, the use of these turbines has not been yet realized for micro hydro applications. Considering the sustainability of micro-hydro power plants, the components of Francis turbine need some simplications so that the manufacturing and operation of the turbine become more feasible. This study focuses on re-designing the turbine with simplications in spiral casing and distributor along with investigating its effects on the performance of runner using CFD. Bovet method is used to obtain meridional dimension of runner while Bladegen feature of ANSYS 15.0 is applied to obtain the runner domain. Optimum design of the runner is obtained by analyzing the effect of parameters like wrap angle, lean angle, blade's beta angle distribution and energy distribution on the runner's performance. The velocity at the runner inlet is very low for micro Francis turbine which increases the dimension of spiral casing so dimension of spiral casing is made small by adjusting guide vane and stay vanes. A comparative study of conventional and simplified design is made based on pressure and tangential velocity distributions along spiral casing and distributor as well as performance of

turbine. It is observed that the required reaction ratio and flow conditions can be obtained by combining the stay vanes and guide vanes. In addition, the proportion of combination depends on the magnitude of reaction ratio. It is found that the combining the stay vane and guide vane gives better result in best efficiency point however at other loading condition efficiency is lower which is due to improper stagnation.

Keywords: Micro Francis turbine, Guide vane, Reaction ratio, Tangential Velocity, Efficiency.

1. Introduction

The energy demand is increasing rapidly with increase in development. The focus for fulfilling this ever increasing energy demand is on renewable energy. There is always a pursuit for finding and implementation of renewable energy source. Hydropower is one of the promising renewable energy sources as well as most established and widely used one for electricity generation and commercial investment. The early generation of electricity from about 1880 often derived from hydro turbines, and the capacity of total worldwide installations has grown at about 5% per year supplying 71% of all renewable electricity worldwide [1].

Francis turbines are widely used turbines in many hydropower projects due to its efficiency and flexibility. It converts both the pressure and kinetic energy retained in water to mechanical energy inside runner thereby producing electrical energy when coupled to the generator. Francis turbines are ideal turbines for the Himalayas and Andes areas where both high and low altitude mountains are located. Past research have shown that more than 60% of installed turbines and up to 80% of hydro turbines required for future installations under Himalayan basins in Nepal will need Francis type of turbine [2].

In Nepal, there are more than 3300 micro hydropower developed so far. However, none of the micro hydro is able to introduce Francis type of turbine although flow and head condition demands this type of turbine. Design and development of Francis turbine is a complex task and requires high engineering effort since turbine needs unique methodology for determined local condition of head and discharge. Therefore, simplifications in design of components of Francis turbine are needed so that the manufacturing and operation of the turbine becomes more feasible and sustainability of micro-hydro power plants can be realised. Re-designing the turbine with simplications in spiral casing and distributor along with investigation of its effects on the performance of runner can be done using CFD [3].

A micro hydropower plant generally runs in isolated system for delivering power to connnected consumers only. This is the reason for the need of higher power output than the power demand of simultaneous consumers in order to avoid overloading condition. In such power scheme control of either flow or load must be very fast and accurate.Governor system is famous in small to large hydropower to control flow for keeping speed and frequency of turbine constant.But, for micro hydro scheme this system is complex and requires high accuracy as well. Therfore, in most of the micro hydropower load control scheme is popular which keeps the turbine output constant irrespective of the demand load. This type of load control is also called electronic governor which keeps the turbine output constant by diverting excess power to sump (i.e. resistors). This type of scheme is simple which has no effect on dynamics of hydraulic system and turbine/generator on stability of governing process as it is free from any inertial effects. For this scheme, distributor system needs to be free of any control mechanism which urges the need of fixed vane distributor [4]. The objective of this study is to address these problems and come up with a simplified design of distributor system which is simple and easy for manufacturing as well as provides required flow condition to runner maintaining reaction ratio. In addition, this study can be utilized for fixed guide vane design for sediment laden water. Clearance gap in guide vane is provided for its operation and due to pressure difference between the high pressure and low pressure side leakage flow is induced. With the erosion in this gap the leakage flow increase which can disturb the main flow causing efficiency drop as well as more erosion in downstream [5]. In order to stop the secondary flow induced by clearance gap, variable speed turbine with fixed vane can be designed and installed in sediment erosion affected regions like Nepal.

2. Design of Distributor

2.1 Design of Guide Vanes

Guide vanes are designed to direct controlled flow of water towards the runner blade allowing control in hydraulic input power. Flow required and pressure conditions of runner are major design criteria of guide vanes. Free vortex flow is considered from guide vane outlet to the runner inlet as there is a conversion between velocity energy and pressure energy only. A free vortex theory can be used as shown in eq. (1)

$$Cu_1 R_1 = Cu_{gvo} R_{gvo} \tag{16}$$

Cu is the tangential component of absolute velocity. The meridional component of absolute velocity is given by eq. (2)

$$Cm_{gvo} = \frac{Q}{2\pi B_{gv} R_{gvo}} \quad [m/s] \tag{17}$$

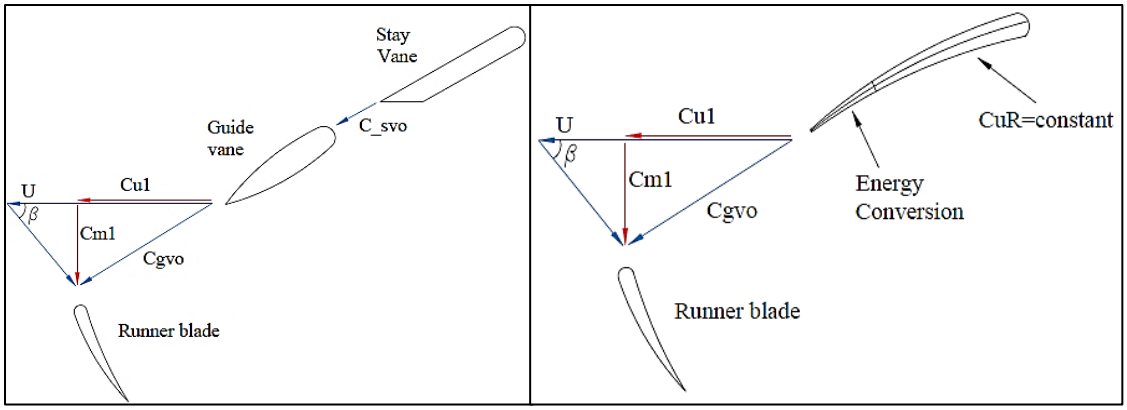

(a) (b)

Fig.1 a) Velocity triangle in conventional turbine b) Velocity triangle in simplified turbine

The outlet angle of guide vane will be same as angle between the inlet tangential and absolute velocities of runner which can be expressed as shown in eq. (3).

$$\alpha_1 = \tan^{-1}\frac{Cm_1}{Cu_1} \tag{18}$$

However, the outlet angle of guide vane needs some correction due to small cross section area at outlet. There are various methods for designing guide vanes. Better direction of flow is given by longer guide vanes. However, frictional loss is more in longer guide vanes and operational requirement determine the shape of guide vanes. The shape affects the distribution of velocity and pressure. Generally, the NACA airfoils are good choice for guide vanes shape. During operation a net rotating torque is experienced so that proper design should be done to ensure timely closure and proper positioning of guide vanes [6].

Diameter of guide vane outlet can be chosen five percent larger than the diameter of runner inlet which is a starting point for guide vane dimensions. The location of guide vane axis diameter is expressed as in eq. (4).

$$D_{ax} = D_1(0.29\Omega + 1.07) \tag{19}$$

D_1 is the diameter of runner inlet and Ω is speed number. Minimum length of guide vane is found by using axis diameter and number of guide vanes required to stop the flow. In order to

prevent the guide vanes to rotate full circle, 10-20% overlap factor is generally used. Length of guide vane is expressed as in eq. (5).

$$L_{gv} = \frac{\pi D_{ax} k_{cf}}{N_{gv}} \tag{20}$$

L_{gv} is the length of guide vane, k_{cf} is the coverage factor and N_{gv} is the number of guide vanes. The diameter of guide vane inlet is calculated by using cosine theorem as expressed in eq. (5).

$$D_{gvi} = 2\sqrt{L_{gv}^2 + \left(\frac{D_{gvo}}{2}\right)^2 - 2L_{gv}\left(\frac{D_{gvo}}{2}\right)\cos\left(\frac{\pi}{2} - \alpha_0\right)} \tag{21}$$

Guide vane axis diameter should be checked and recalculated using cosine theorem if guide vane axis is too close to guide vane outlet. Generally, axis is located at 2/3 of guide vane length from outlet [6].

2.2 Design of Stay vanes

Stay vanes are designed to withhold forces from the pressure acting on spiral casing and have no hydraulic effect. For simplicity, the area in which pressure acts can be assumed an annulus with constant inner and outer diameter as of inlet spiral case. At full load condition diameter of stay vane outlet is 1-5% greater than guide vane inlet diameter [6]. Free vortex assumption is made in the flow through the gap; flow through stay vane and throughout spiral case as expressed in eq. (7)

$$Cu_{gvi} R_{gvi} = Cu_{svo} R_{svo} = \text{constant} \tag{22}$$

Determination of optimal length of a stay vane is an iterative process. Initially diameter of stay vane inlet is chosen. Minimum length of stay vane is expressed as in eq. (8)

$$L_{sv} = \frac{F_{max}}{\sigma_{steel} t_{sv} Z_{sv}} \tag{23}$$

Fmax is the maximum force due to water head on the spiral casing, σ steel is the strain property of the material, Zsv is the number of stay vanes, tsv is the thickness of stay vane. For BEP equal number of guide vanes and stay vanes should be chosen. Thick stay vanes will disturb the flow pattern and decrease in flow area [6]. These two concerns should be a compromise.

Dsvi is obtained forming stay vane as free vortex streamline. New Dsvi is used to calculate new spiral case that gives new area of annulus for next iteration step. The leading edge and trailing edge of stay vane should be designed to disturb the flow minimally. As stay vanes have

thickness flow area decreases so that in order to compensate the trailing edge angle should be chosen to be 30 degrees. Leading edge can be defined as a half circle. Minimum thickness for stay vane is about 2mm [6].

2.3 Design of Spiral Casing

Flow in each section of spiral casing is determined from the fact that constant water flow must be provided from spiral casing to the stay vane. Dimensions of all the section is calculated with the help of constant circulation 'Ct' using iterative process. The iteration is carried out to match required vortex at inlet of vane and computed vortex at spiral casing [6].

$$C_t = \frac{Q}{2 \cdot r^2 \int_{\varphi_\circ}^{\pi} \left(\frac{\sin^2 \varphi}{R_T - r \cdot \cos\varphi} \right) d\varphi} \tag{24}$$

$$C_u = \frac{Q}{R \cdot 2 \cdot r^2 \int_{\varphi_\circ}^{\pi} \left(\frac{\sin^2 \varphi}{R_T - r \cdot \cos\varphi} \right) d\varphi} \tag{25}$$

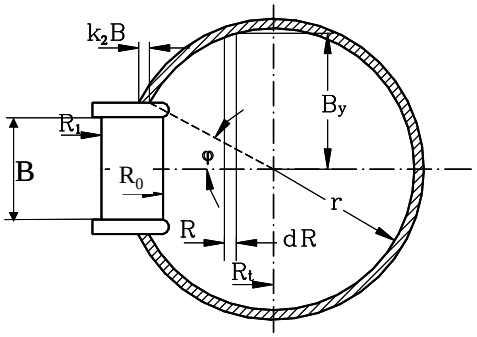

Fig. 2 Circular cross section of spiral [6]

Conventional design of the guide vane, stay vane and spiral casing for micro hydro with low and medium head results in big spiral casing which can result in very low velocity requirement at inlet section of spiral casing. These can cause an increase in overall dimension of water convey system as well as power house. However, simplification in distribution system without any change in the inlet condition of runner can be achieved by combining stay vane and guide vane in certain proportion. The velocity and pressure distribution in vanes and spiral can be controlled to make the dimension of casing within limit and without altering inlet condition required for the runner. In present study, the vane which is combination of 20 percent of guide vane and 80 percent of stay vane is fixed at best stagnation angle as shown in figure. This proportion is selected after observation of the flow behavior in vanes at different combination.

Main focus is given to maintain the required reaction ratio and tangential velocity distribution at runner inlet. The length of stay section is chosen in order to obtain the flow condition at spiral casing outlet which is dependent on pressure head available. It is assumed that the flow velocity at spiral casing inlet is 12% to 25% of velocity [7] given by

$$C = \sqrt{(2gH)} \tag{26}$$

Reaction ratio along with specific speed plays an important role in determination of blade loading and for cavitation performance of a reaction turbine. The ratio of pressure drop form runner inlet to outlet and total available head at best efficiency points for cu2=0 gives the reaction ratio.

$$\underline{h}_1 - \underline{h}_2 = \frac{h_1 - h_2}{H} \tag{27}$$

$$\underline{h}_1 - \underline{h}_2 = 2\underline{u}_1\underline{c}_{u1} - \underline{c}_{u1}^2 \tag{28}$$

Where, $\underline{h}_1$ and $\underline{h}_2$ is reduced pressure head at inlet and outlet of runner

$\underline{u}_1$ is reduced peripheral velocity

$\underline{c}_{u1}$ is reduced tangential velocity at runner inlet

H is total head.

3. Numerical Model

The conventional computational domain consists of spiral casing, stay vanes, guide vanes, runner and draft tube while in simplified domain spiral casing; fixed vanes, runner and draft tube are used. Meshing of runner is carried out in turbo grid which consists of hexahedral elements. For all other components, unstructured tetrahedral meshing is used due to its flexibility and easiness while meshing. Effect of walls on boundary layer flow is captured with smooth flow of 8 layers of inflation with growth rate of 1.2 as shown in figure. Mesh independence test is carried to ensure there is little influence of grid number on results computed. The mesh independence test is carried out taking tangential velocity at out of vane which is shown in figure.

For numerical solution, turbulence simulation based on Reynolds-Average Navier Stroke (RANS) is used. RANS is based on continuity equation and momentum equation as described as follows.

$$\frac{\partial U_i}{\partial x_i} = 0 \tag{29}$$

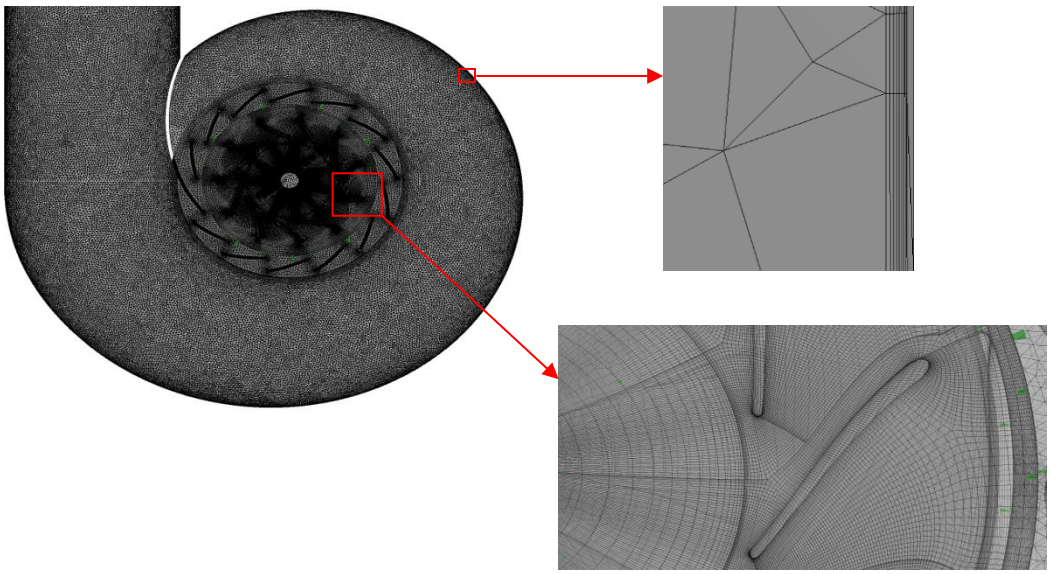

Figure. Meshing for the computational domain [8]

$$\frac{\partial U_i}{\partial t} + U_j \frac{\partial U_i}{\partial x_j} = -\frac{1}{\rho}\frac{\partial P}{\partial x_i} + \frac{\partial}{\partial xj}\left[\nu\left(\frac{\partial U_i}{\partial x_j} + \frac{\partial U_j}{\partial x_i}\right) - \overline{u'_i u'_j}\right] \tag{30}$$

Where, U, u', P, v and ρ are velocity, fluctuating value of velocity, pressure, kinematic viscosity and density, respectively.

In present study, k-epsilon turbulence model is used for initial solution as well as comparative study as this model needs less computational effort. K-epsilon model have robustness, reasonable accuracy and economy this model is very popular for much application. This is a

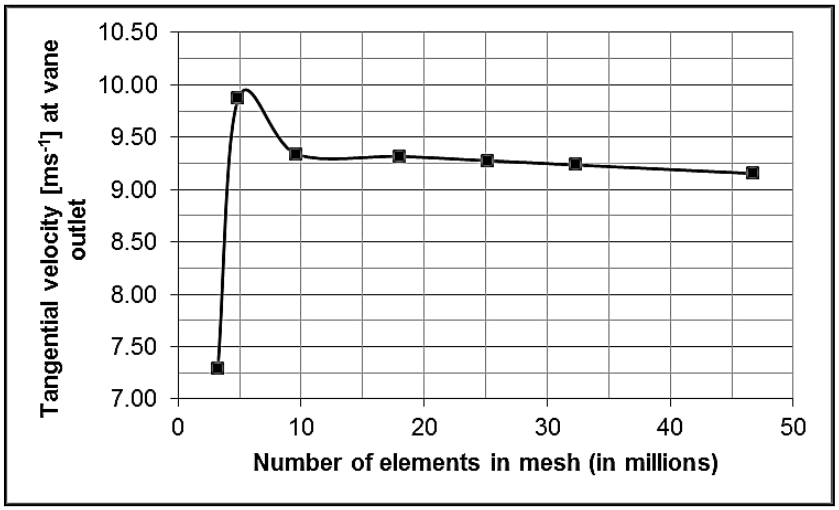

Figure . Meshing independence test for circular cross section [8]

two equation method in which turbulent kinetic energy is expressed by k and the dissipation rate of k by ε.

$$\frac{\partial k}{\partial t}+U_i\frac{\partial k}{\partial x_i}=\frac{\partial}{\partial x_i}\left(\frac{\nu_t}{\sigma_k}\frac{\partial k}{\partial x_i}\right)+\nu_t\left(\frac{\partial U_i}{\partial x_j}+\frac{\partial U_j}{\partial x_i}\right)\frac{\partial U_i}{\partial x_j}-\varepsilon \tag{31}$$

$$\frac{\partial \varepsilon}{\partial t}+U_i\frac{\partial \varepsilon}{\partial x_i}=\frac{\partial}{\partial x_i}\left(\frac{\nu_t}{\sigma_\varepsilon}\frac{\partial \varepsilon}{\partial x_i}\right)+c_{1\varepsilon}\frac{\varepsilon}{k}\nu_t\left(\frac{\partial U_i}{\partial x_j}+\frac{\partial U_j}{\partial x_i}\right)\frac{\partial U_i}{\partial x_j}-c_{2\varepsilon}\frac{\varepsilon^2}{k} \tag{32}$$

Flow through the turbine is considered to be incompressible, viscous and fully turbulent. Total pressure at spiral casing inlet based on nominal head and nominal mass flow rate at draft tube outlet is used as boundary condition for simulation. Runner is considered as rotational domain with 1500 rpm while all other components are stationary. Since, the vanes are fixed flow rates are changed from 80 % to 120% of design flow to obtain efficiency at different flow condition for simplified turbine.

4. Results and Discussion

Pressure distribution, tangential velocity distribution and reaction ratio at outlet of vane are studied. Efficiency of simplified turbine is studied for different flow rates and is compared with the conventional turbine without simplification. In this study, head is made constant by using pressure equivalent to nominal head at inlet of spiral casing. However, the dimension of the spiral casing for simplified turbine is smaller than the conventional turbine. Reaction ratio of the turbine is calculated for the runner which is 0.626. This means up to runner inlet only 37.4% of pressure head is converted to velocity head by the guide vane and 62.6% of pressure head is available for runner.

Static pressure contour at horizontal mid plane of the simplified turbine and conventional turbine with spiral casing and distributor is shown in Figure. It can be observed that the pressure at guide vane outlet in case of conventional turbine is lower than that of simplified which may be due to pressure loss at stay vane, space between stay vane and guide vane. Also, pressure at inlet section is higher for conventional turbine due to low velocity resulting from larger dimensions of spiral casing. Reaction ratio at guide vane outlet obtained for conventional and simplified turbine at best efficiency point is 0.589 and 0.659 respectively. There is 1.62 m difference in head between the two turbines which may be the cause of difference in reaction ratio. The reactions ratios obtain from numerical analysis are comparable to the result obtained from analytical calculation which is 0.626. Ho It can be observed from Figure that water is

accelerated more through the guide vanes in conventional turbine as the length of guide vane is longer than that of simplified turbine which may be the cause for lower ratio reaction.

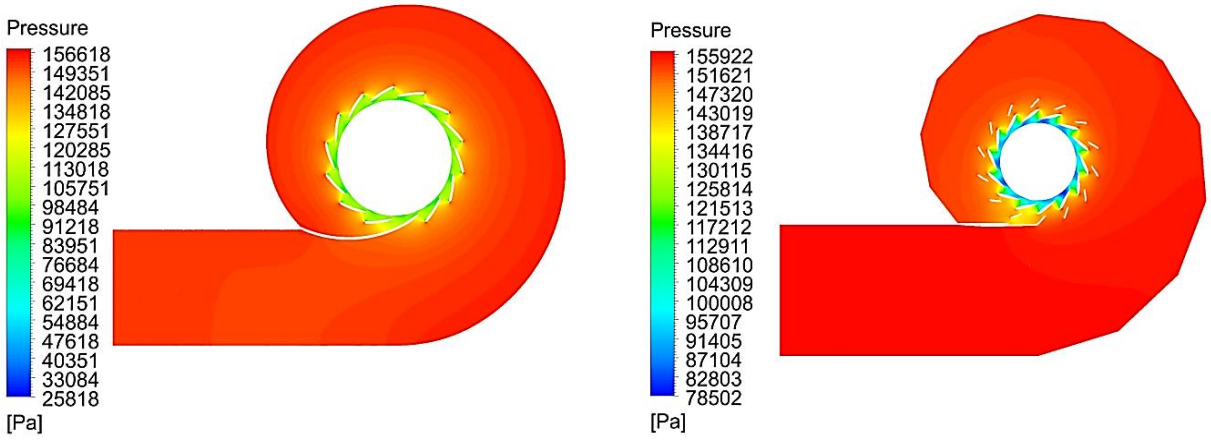

Figure . Static pressure contour at mid plane (a) Simplified (b) Conventional

Tangential velocity distribution at outlet of guide vane for conventional turbine and simplified turbine are plotted along with analytical result against periodic angular position. There is fluctuating numerical results in comparison to analytical results as CFD over predict wakes and analytical results are ideal results without any viscous and frictional effect. It is can be observed that there is no significant difference in distribution of tangential velocity of both the design however distribution in conventional design is a better than the simplified design.

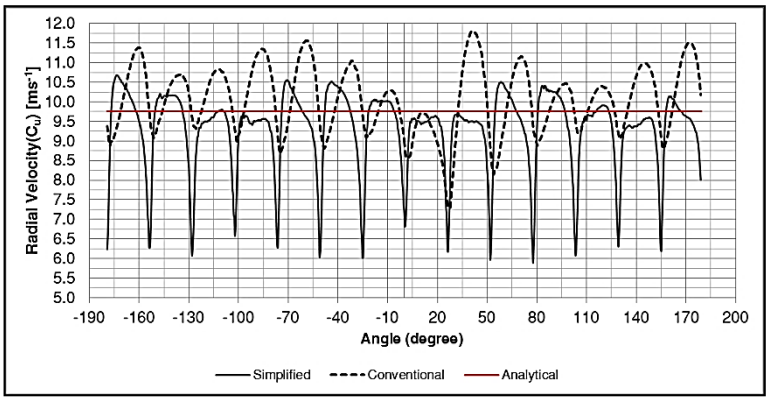

Figure. Tangential velocity distribution at vane outlet

Hydraulic efficiency obtained from numerical study at best efficiency point is 90.2% for simplified turbine and 86.15% for conventional turbine. The lower efficiency in conventional turbine may due to the losses in stay vanes and guide vane as their length is larger than the vane

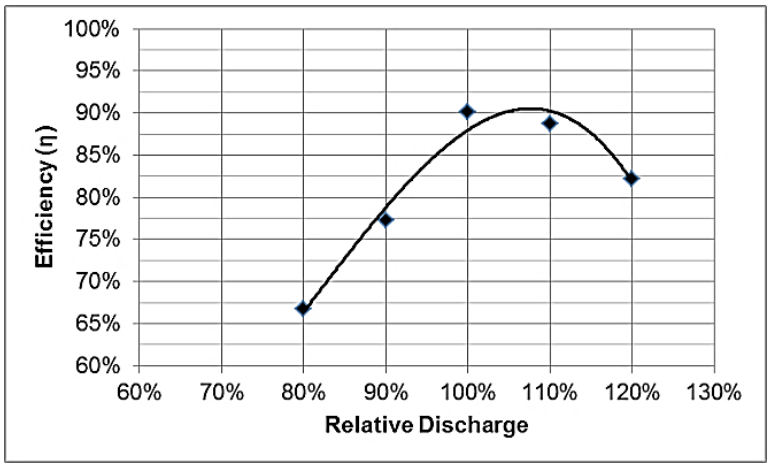

Figure. Tangential velocity distribution at vane outlet

of simplified turbine. Figure shows efficiency for different discharge. The vane in the simplified designed is fixed at angle corresponding to best efficiency point which will create incorrect stagnation at full load and part load causing steeper efficiency curve towards the part and full load as observed in figure.

5. Conclusion

In this paper, distributor and spiral casing for conventional and simplified were designed and numerically compared. Distribution of pressure and tangential velocity along with the efficiency of both the design are compared. It is seen that by combining the stay vane and guide vane in certain proportion required flow condition and reaction ratio can be achieved. The proportion of combination depends on the degree of conversion of pressure head to velocity head which is greatly influenced by the types of Francis turbine. For high head Francis turbine the conversion needed is higher demanding greater percentage of guide vane in the combination while in low head turbine conversion required is low demanding lower percentage of guide vane in the combination. The turbine used in this study falls in low head region so only 20% of guide vane portion give good combination with comparable results. Comparison of tangential velocity at guide vane outlet revealed that simplified design can provide required flow condition for runner. At best efficiency point, the efficiency of simplified turbine is better than the conventional turbine. However, efficiency in part load and full load have steep slope due to improper stagnation angle which can cause flow separation and losses. For fixed vane

distributor system, runner should be designed with flexibility in stagnation so that it gives better performance in both part load and full load condition.

It is concluded from this study that dimension of spiral casing as well as distributor can be reduced by combining stay vane and guide vane without significant effect in flow condition required for runner. Also, this system is suitable for micro hydro with electronic load controller and hydro turbine operating in sediment laden water.

References

[1] World Energy Council, 2016, “World Energy Resources 2016”, WE Council, London

[2] Panta, S., Lamsal M., Thapa B. S. and Thapa B., 2014, "Predication of turbine needed for future hydropower project in Nepal," Hydro Nepal, Journal of Water, Energy and Environment, Vol. 14.

[3] Ghimire, A., Dahal, D. R., Pokherel, N., Chitrakar, S., Thapa, B.S. and Thapa, B., 2019, “Opportunities and challenges of introducing Francis turbine in Nepalese micro hydropower projects", International Symposium on Current Research in Hydropower Technologies (CRHT-IX), Dhulikhel, Nepal.

[4] Fischer, G., Arter, A., Meier, U. and Chapallaz, J. M., 1990, Harness water power in small scale: governor product information, SKAT, Switzerland.

[5] Chitrakar, S., Dahlhaug, O.G. and Neopane, H. P., 2018, “Numerical investigation of the effect of leakage flow through erosion-induced clearance gaps of guide vanes on the performance of Francis turbines”, Taylor & Francis, Vol. 12, No. 1, pp. 662–678.

[6] NTNU, 2008, “High Pressure Hydraulic Machinery”, Course Reports, NTNU, Norway.

[7] Krishna, H. R, 1997, “Hydraulic Design of Hydraulic Machinery”. Ashgate Publishing Limited, United Kingdom.

[8] Dahal, D. R., Chitrakar, S., Kapali A., Thapa, B.S., and Neopane, H.P., 2019, “Design of spiral casing of Francis turbine for micro hydro applications", International Symposium on Current Research in Hydropower Technologies (CRHT-IX), Dhulikhel, Nepal.

[9] Choi, Y. H., Zullah, M.A., Roh H.W., Ha, P.S., Oh, S. Y. and Lee, Y.-H., 2012, “CFD validation of performance improvement of a 500 kW Francis turbine,” Renew. Energy, Vol. 54, pp. 111–123.

[10]Teran, L.A., Larrahondo, F.J. and Rodriguez, S.A., 2016, Performance improvement of a 500-kW Francis turbine based on CFD”, Renew. Energy, Vol. 96, pp. 977–992.

[11] Ayli, E., Celebioglu, K., and Aradag, S., 2016, “Determination and generalization of the

effects of design parameters on Francis turbine runner performance," Eng. Appl. Comput. Fluid Mech., Vol. 10, No. 1, pp. 545–564.

[12] Nakkina, P. R., Prakash, K. A., and Kumar, G. S. , 2016, "Numerical studies on fluid flow characteristics through different configurations of spiral casing," Eng. Appl. Comput. Fluid Mech., Vol. 10, No. 1, pp. 297–311.

[13] Alnaga, A. and Kueny, J., 2010 , "Optimal design of hydraulic turbine distributor", Vol. 3, No. 2, pp. 175–185.

[14] Odesola, I. F. and Oririabre, J. I., 2013, "Development of a 5kw Francis turbine Runner using computation fluid dynamics",

[15] Thapa, B.S, Dahlhaug, O.G., and Thapa, B., 2018, Flow measurements around guide vanes of Francis turbine: A PIV approach, Renew. Energy, Vol. 126, March, pp. 177–188.

Acknowledgments

This study was a part of MS by Research at Turbine Testing Lab (TTL) in Kathmandu University. The research program is funded by EnergizeNepal Project at TTL. Authors would like to thank TTL, Aatmaram Kayastha, Aman Kapali, Amul Ghimire, Rabina Awal, Prajwal Sapkota and Nischal Pokharel for their continuous help and support.

APPENDIX II

Experimental Setup

Figure Experimental Setup

Figure VFD

Figure Torque Transducer

Figure Pressure Sensor

Figure Flowmeter

Figure Data Logger

	A	B	C	D	E	F	G	H	I	J	K	L	M	N
1	S.N.	Weight no	Weight (gm)	Cumulative Weight (gm)	Arm Length (m)	Torque (Nm)	Voltage onload	Voltage offload	Voltage onload	Voltage offload	Hysteresis			
2	1	0		0	0.49886	0.00	0.0060	0.0058	0.0063	0.0057	0.0002		0.0000	0.00604
3	2	5	493.075	493.075	0.49886	2.41	0.0448	0.0458	0.0452	0.0449	-0.0011		2.4130	0.04477
4	3	7	502.454	995.529	0.49886	4.87	0.0991	0.0992	0.0458	0.0983	-0.0002		4.8719	0.09906
5	4	19	495.168	1490.697	0.49886	7.30	0.1510	0.1516	0.1515	0.1517	-0.0006		7.2952	0.15096
6	5	17	504.512	1995.209	0.49886	9.76	0.2023	0.2026	0.2030	0.2023	-0.0003		9.7642	0.20231
7	6	21	518.863	2514.072	0.49886	12.30	0.2543	0.2542	0.2545	0.2544	0.0001		12.3034	0.25434
8	7	1	520.535	3034.607	0.49886	14.85	0.3060	0.3056	0.3061	0.3060	0.0005		14.8508	0.30603
9	8	15	461.92	3496.527	0.49886	17.11	0.3514	0.3514	0.3521	0.3515	-0.0001		17.1114	0.35135
10	9	2	503.978	4000.505	0.49886	19.58	0.4016	0.4014	0.4017	0.4015	0.0003		19.5777	0.40163
11	10	3	476.628	4477.133	0.49886	21.91	0.4488	0.4485	0.4486	0.4484	0.0003		24.3455	0.49829
12	11	12	497.615	4974.748	0.49886	24.35	0.4983	0.4979	0.4982	0.4978	0.0004		26.7455	0.54677
13	12	22	490.419	5465.167	0.49886	26.75	0.5468	0.5465	0.5463	0.5467	0.0003		29.1753	0.59621
14	13	9	496.501	5961.668	0.49886	29.18	0.5962	0.5954		0.5957	0.0008		31.6944	0.64714
15	14	14	514.758	6476.426	0.49886	31.69	0.6471	0.6464	0.6463	0.6463	0.0008			
16	15	11	509.586	6986.012	0.49886	34.19	0.6471	0.6965	0.6966	0.6967	-0.0494		36.8283	0.75068
17	16	13	539.471	7525.483	0.49886	36.83	0.7507	0.7499	0.7499	0.7492	0.0008		39.3685	0.8017
18	17	20	519.062	8044.545	0.49886	39.37	0.8017	0.8010	0.8012	0.8011	0.0007		41.7893	0.85009
19	18	6	494.668	8539.213	0.49886	41.79	0.8501	0.8500	0.8499	0.8497	0.0001		44.1760	0.8986
20	19	8	487.685	9026.898	0.49886	44.18	0.8986	0.8982	0.8982	0.8976	0.0004		46.6159	0.94771
21	20	16	498.581	9525.479	0.49886	46.62	0.9477	0.9469	0.9472	0.9471	0.0008		48.9536	0.99499
22	21	18	477.683	10003.16	0.49886	48.95	0.9950	0.9945	0.99437	0.9945	0.0005			

Figure Instrument Calibration

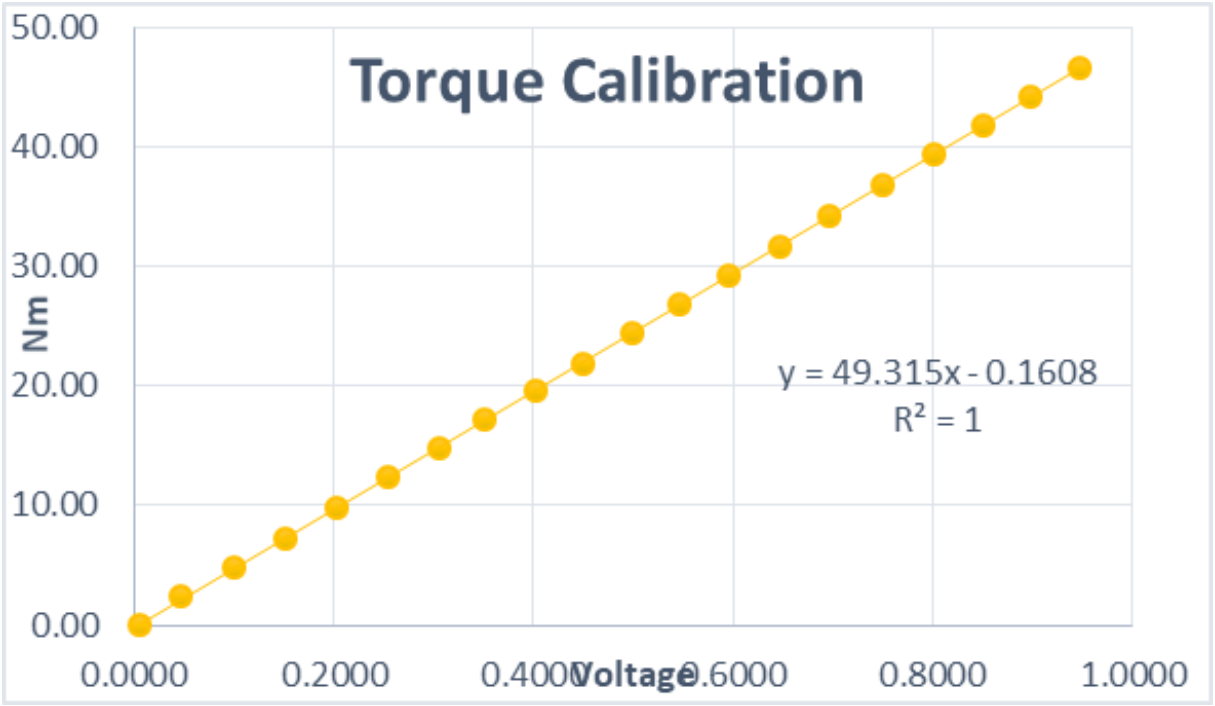

Figure Torque Calibration

APPENDIX III

Design Tool

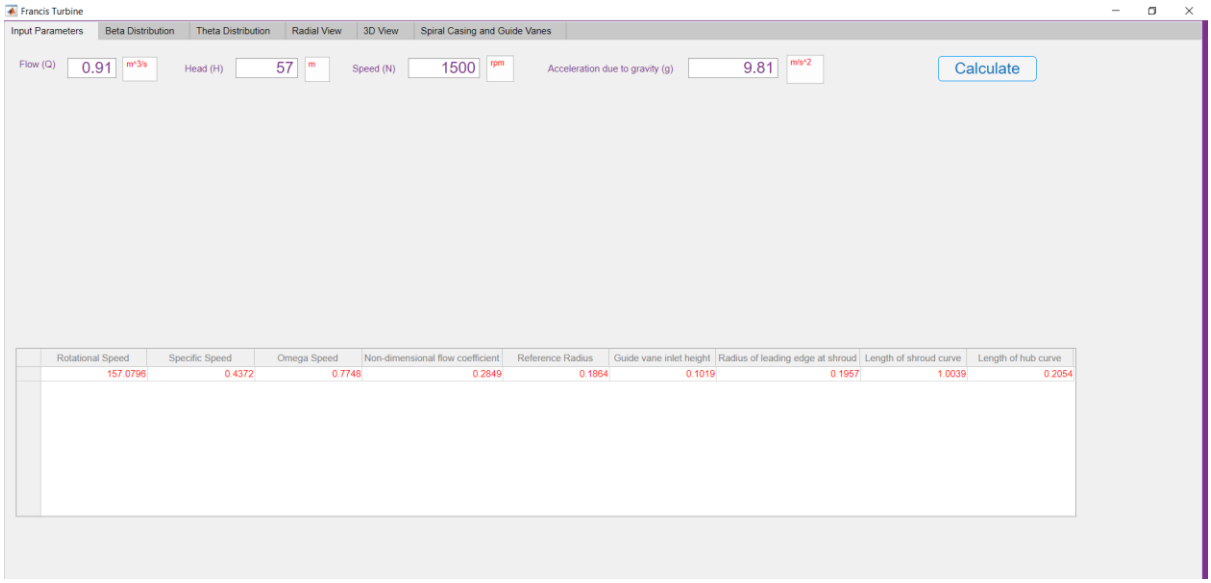

Figure Tab 1: Input Parameters

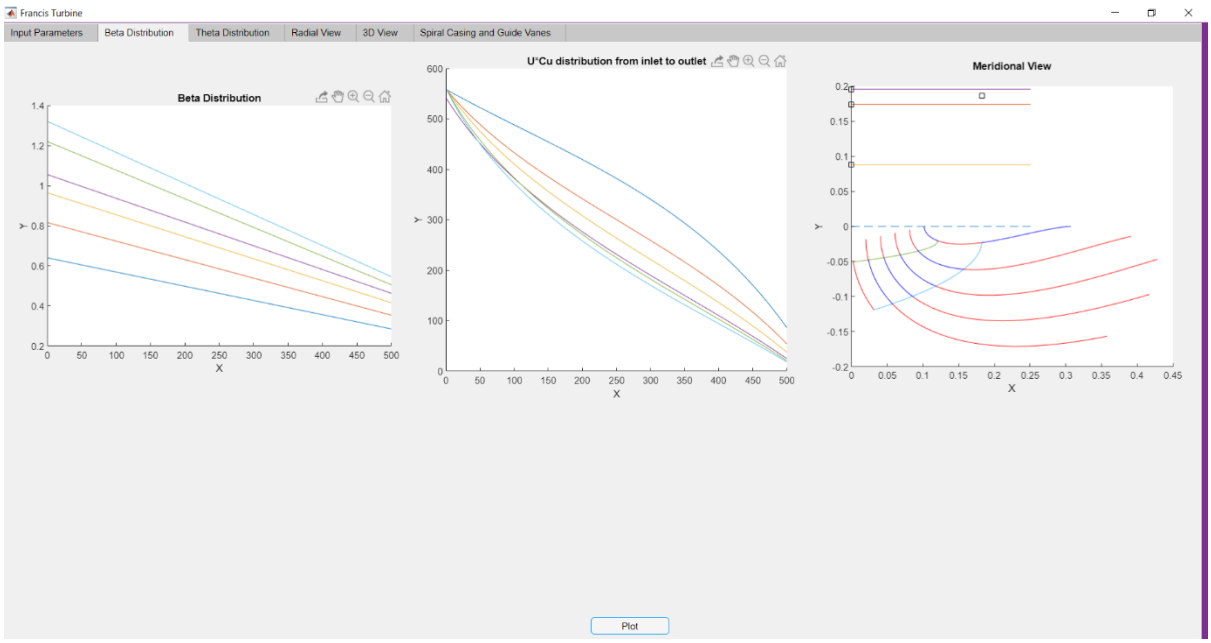

Figure Tab 2: Beta Distribution

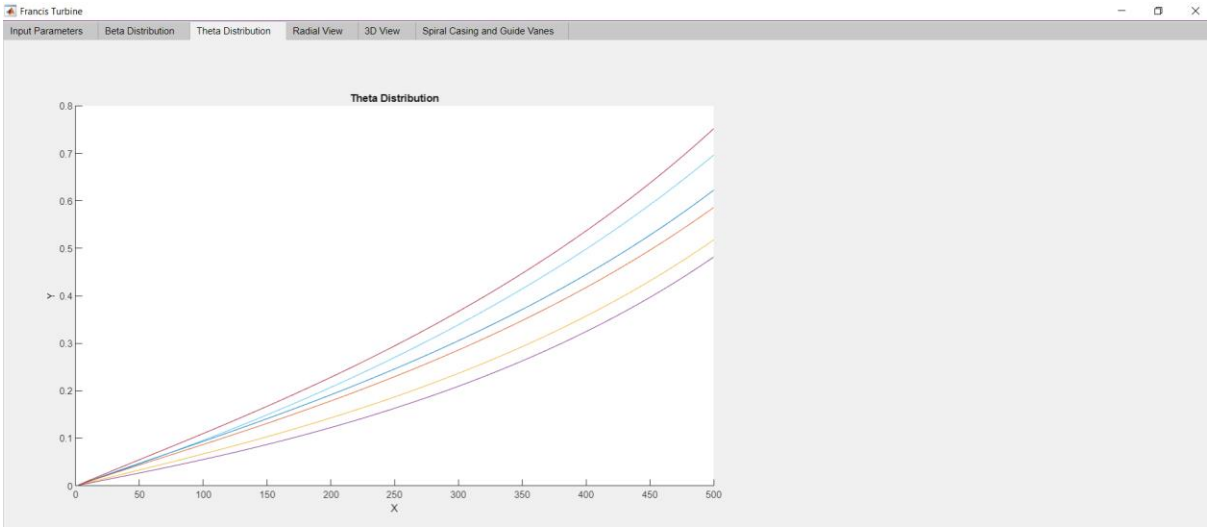

Figure Tab 3: Theta Distribution

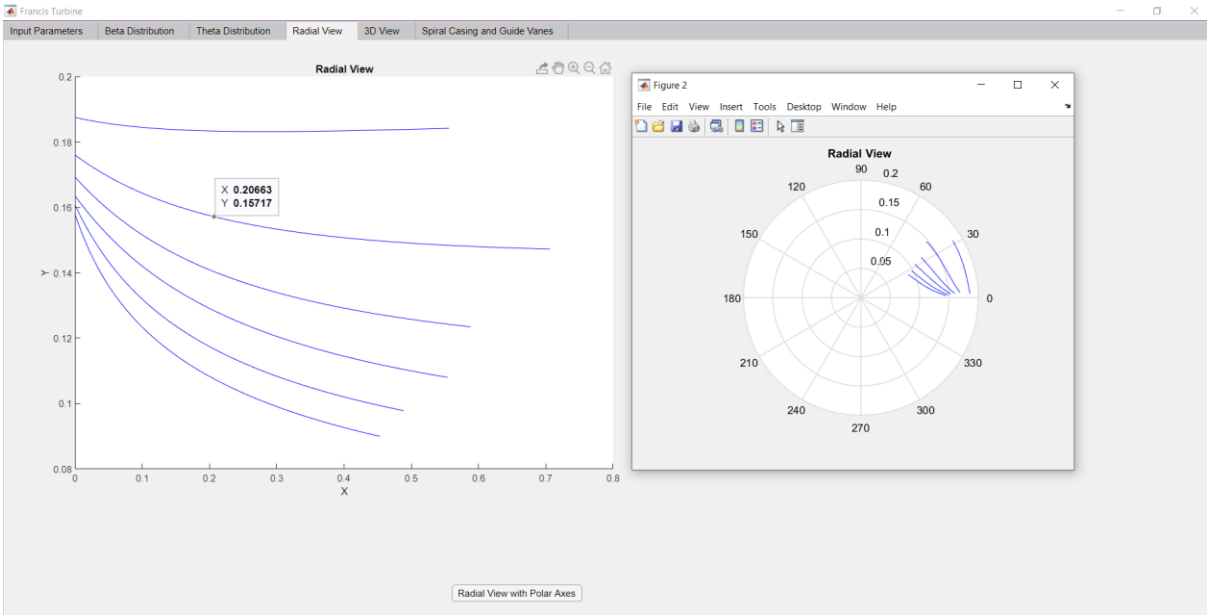

Figure Tab 4: Radial View

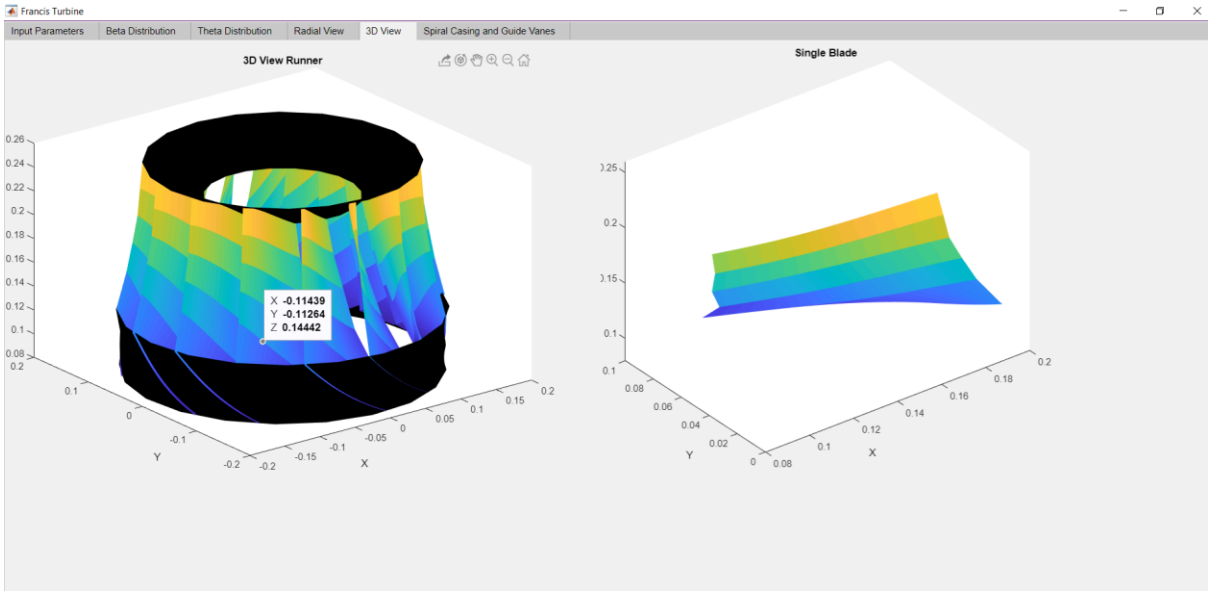

Figure Tab 5: 3D View

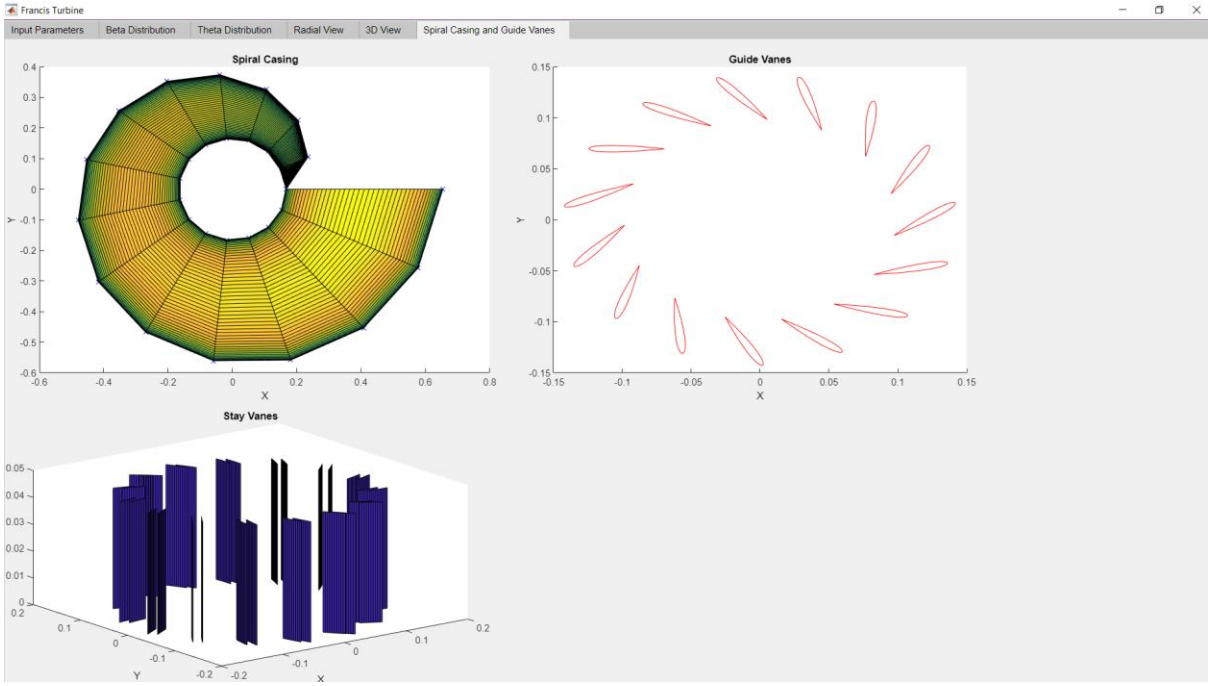

Figure Tab 6: Spiral Casing and Guide Vanes